Metals **2014**, *4*, 168-195; doi:10.3390/met4020168

OPEN ACCESS

metals

ISSN 2075-4701

www.mdpi.com/journal/metals/

Article

Phase Equilibria of the Ce-Mg-Zn Ternary System at 300 °C

Ahmad Mostafa and Mamoun Medraj *

Department of Mechanical and Industrial Engineering, Concordia University,
1455 de Maisonneuve Blvd. West, Montreal, QC H3G 1M8, Canada;
E-Mail: ah_mosta@encs.concordia.ca

* Author to whom correspondence should be addressed; E-Mail: mmedraj@encs.concordia.ca;
Tel.: +1-514-848-2424 (ext. 3146); Fax: +1-514-848-3175.

Received: 10 April 2014; in revised form: 13 May 2014 / Accepted: 15 May 2014 /
Published: 28 May 2014

Abstract: The isothermal section of the Ce-Mg-Zn system at 300 °C was experimentally established in the full composition range via diffusion multiple/couples and key alloys. Annealed key alloys were used to confirm the phase equilibria obtained by diffusion multiple/couples and to determine the solid solubility ranges. Spot analysis was carried out, using wavelength dispersive X-ray spectroscopy (WDS), to identify the composition of the observed phases. The composition profiles were obtained using WDS line-scans across the diffusion zones. X-ray diffraction (XRD) was performed to identify the phases in the annealed alloys and to confirm the WDS results. Eight ternary compounds, in the Ce-Mg-Zn isothermal section at 300 °C, were observed from 45–80 at.% Zn. These are: τ_1 ($Ce_6Mg_3Zn_{19}$), τ_2 ($CeMg_{29}Zn_{25}$), τ_3 ($Ce_2Mg_3Zn_3$), τ_4 ($CeMg_3Zn_5$), τ_5 ($CeMg_7Zn_{12}$), τ_6 ($CeMg_{2.3-x}Zn_{12.8+x}$; $0 \leq x \leq 1.1$), τ_7 ($CeMgZn_4$) and τ_8 ($Ce(Mg_{1-y}Zn_y)_{11}$; $0.096 \leq y \leq 0.43$). The ternary solubility of Zn in the Ce-Mg compounds was found to increase with a decrease in Mg concentration. Accordingly, the ternary solid solubility of Zn in $CeMg_{12}$ and $CeMg_3$ was measured as 5.6 and 28.4 at.% Zn, respectively. Furthermore, the CeMg and CeZn showed a complete solid solubility. The complete solubility was confirmed by a diffusion couple made from alloys containing CeMg and CeZn compounds.

Keywords: Ce-Mg-Zn system; diffusion couples; diffusion multiple; experimental investigation; ternary phase diagram

---

1. Introduction

Casting magnesium alloys exhibit low mechanical strength and ductility, and Mg alloys, in general, are limited to certain applications, because of their poor plastic properties at room temperature and poor creep resistance at elevated temperatures [1]. Thus, the development of Mg alloys with high mechanical properties becomes essential for many applications. Zn is one of the potential alloying elements added to Mg to improve its mechanical properties and corrosion resistance [2]. The problem with the Mg-Zn binary alloys is the low melting point, deeming these alloys not suitable for elevated temperature applications. In order to improve the mechanical properties at elevated temperatures, rare earth (RE) elements are added to form precipitates by age hardening [3], on the one hand. On the other hand, the addition of rare earth elements can also refine the grains and form stable compounds with a high melting point [4]. Cerium, as a major component of the mischmetal, is considered one of the most important additives to modify the Mg-Zn binary alloys [5], because it forms a series of stable intermetallic compounds.

Diffusion couples are valuable experimental techniques for phase diagram studies. They are subjected to the assumption of the local equilibria in the diffusion zone, where the diffusion reaction takes place [6]. Thin layers in thermodynamic equilibrium are formed adjacent to one another. The phase equilibria, then, can be depicted via the diffusion paths across these layers [7]. In this work, diffusion couples and one diffusion multiple were used to understand the phase relationships in the Ce-Mg-Zn isothermal section at 300 °C. Key alloys, used to verify the phase relations obtained from diffusion paths and to study the regions that were not covered by the diffusion couples, were analyzed using X-ray powder diffraction (XRD), energy dispersive X-ray spectroscopy (EDS), wavelength dispersive X-ray spectroscopy (WDS) and scanning electron microscopy (SEM).

2. Literature Review

The solubility of Ce and Zn in Mg in the Ce-Mg-Zn system was first studied by Korolkov and Sal`dau [8] using XRD, thermal and microstructural analysis. Thermal analysis results were used to construct six vertical sections with a mass ratio of Ce:Zn of 5:1, 2:1, 1:1, 1:2, 1:4.5 and 1:10 and to draw the liquidus surface near the Mg-rich corner. On the other hand, the microstructural studies were used to determine the combined solubility of Ce and Zn in Mg in the furnace cooled samples and those annealed at 200, 300 and 335 °C. Korolkov and Sal'dau [8] reported an invariant reaction at 50 at.% Mg-47.5 at.% Zn-2.5 at.% Ce occurring between 341 and 343 °C, without giving further explanations on the reaction type. The partial phase diagram, shown in Figure 1a, was investigated by Melnik *et al*. [9] in the region of Mg-$MgZn_2$-CeMg-CeZn at 300 °C using XRD. Four ternary compounds were discovered, τ_1 ($CeMg_7Zn_{12}$), τ_2 ($Ce(Mg,Zn)_{10.1}$), τ_3 ($CeMg_3Zn_5$) and τ_4 ($Ce(Mg,Zn)_3$). τ_2 and τ_4 showed extended solubility ranges from 9.1 to 45.5 at.% Zn and from 35 to 45 at.% Zn at 300 °C, respectively. The crystal structures of τ_1 and τ_3 are unknown. They [9] suggested the existence of a wide two-phase region between the ternary solid solutions extending from $CeMg_{12}$ up to 40 at.% Zn and Ce_3Mg up to 48 at.% Zn at 300 °C. However, these findings have not been confirmed experimentally, yet. Drits *et al*. [10], using XRD, differential thermal analysis (DTA), EPMA and microstructural analysis, constructed two vertical sections in the Mg-rich corner, at 24 wt.% Zn and

34 wt.% Zn, both from 0 to 20 wt.% Ce. Two ternary compounds were confirmed using X-ray analysis; these compounds are: $CeMg_7Zn_{12}$ and $Ce(Mg_{0.2–0.3}Zn_{0.1–0.3})_{10.1}$. In addition, two invariant reactions, L + $Ce(Mg_{0.2–0.3}Zn_{0.1–0.3})_{10.1}$ ↔ (α-Mg) + $CeMg_7Zn_{12}$ at (349 ± 1) °C and L ↔ (α-Mg) + $CeMg_7Zn_{12}$ + $Mg_{51}Zn_{20}$ at (341 ± 1) °C, were detected.

Later, Kolitsch *et al*. [11] re-evaluated the partial isothermal section constructed by Melnik *et al*. [9] at 300 °C. In their review, the tie line between τ_1 and $Mg_{51}Zn_{20}$ was omitted, because $Mg_{51}Zn_{20}$ is not considered stable at 300 °C [12]. Kevorkov and Pekguleryuz [13] studied the Ce-Mg-Zn phase diagram at 350 °C, shown in Figure 1b, by means of diffusion couples and SEM/EDS analysis. As a starting point, they [13] used the isothermal section constructed by Kolitsch *et al*. [11] at 300 °C. Two new ternary compounds, labeled as Phase 2 ($Ce_{1.82}Mg_{53.14}Zn_{45.04}$) and Phase 6 ($Ce_{6.21}Mg_{14.56}Zn_{79.23}$), were observed. In addition, the solid solubilities of the ternary solid solutions were determined using EDS/EPMA techniques. Several tie-lines were not certainly recognized in the work of Kevorkov and Pekguleryuz [13]. These tie-lines were indicated as dashed-lines in the Ce-Mg-Zn isothermal section at 350 °C. Furthermore, the phase relationships with the Ce-Zn compounds were not well determined. Chiu *et al*. [14], using thermodynamic modeling and experimental investigation, studied the solubility ranges and the invariant reactions in the Mg-rich corner (34–85 at.% Mg) at 300 °C. Their aim was to find the missing key data for their model using DSC, DTA and SEM/EDS techniques. They recalculated a ternary eutectic L → MgZn + Mg_7Zn_3 + τ_2 (τ_2-$CeMg_{29.2}Zn_{24.8}$) at ~341 °C with 2.5 at.% Ce in the liquid. The calculated eutectic temperature [14] was very close to the temperature reported by Korolkov and Sal'dau [8] at 342 °C; although, Kevorkov and Pekguleryuz [13] studied the system at 350 °C. However, they [13] did not report any liquid at that temperature. Later, Huang *et al*. [1] studied the phase relationships in the Ce-Mg-Zn system, near the Mg-rich corner, at 350 °C; using SEM/EPMA, XRD, selected area electron microscopy (SAED) and transmission electron microscopy (TEM). One linear ternary compound (*T*-phase), containing 7.7 at.% Ce and 19.3–43.6 at.% Zn, in equilibrium with (α-Mg) and (α-Mg) + $Ce_{1.8}Mg_{55}Zn_{43.2}$, was observed. The *T*-phase was designated as $Ce(Mg_{1-x}Zn_x)_{11}$; x = 0.096–0.43 at.%, which is different from the extended solid solution $Ce(Mg_{1-x}Zn_x)_{12}$; x = 0–0.078 at.%. The crystal structure was reported as *C*-centered orthorhombic with lattice parameters of a = 0.96–1.029 nm, b = 1.115–1.204 nm and c = 0.94–1.015 nm. Recently, the crystal structures, compositions and phase relationships in the Ce-Mg-Zn system were identified at 400 °C by Huang *et al*. [5]. The *T*-phase was found in equilibrium with the liquid phase at 400 °C. Thus, the phase equilibria of (α-Mg) + ($CeMg_{12}$), (α-Mg) + *T*-phase, (α-Mg) + *T*-phase + liquid and (α-Mg) + *T*-phase + ($CeMg_{12}$) were identified. The maximum solubility of Zn in $CeMg_{12}$ was measured to be 7.8 at.% Zn. More recently, Pavlyuk *et al*. [15] established the Ce-Mg-Zn isothermal section at 197 °C, shown in Figure 1c, using single crystal XRD and EPMA techniques. Seven ternary compounds, namely τ_1 ($Ce(Mg_{0.137}Zn_{0.863})_{11}$), τ_2 ($CeMg_{29.2}Zn_{24.8}$), τ_3 ($CeMg_{1+x}Zn_{2-x}$; x = 0.48), τ_4 ($CeMg_{2.5}Zn_{4.5}$), τ_5 ($Ce_3Mg_{13}Zn_{30}$), τ_6 ($CeMg_{2.3-x}Zn_{12.8+x}$; x = 0.11) and τ_7 ($Ce_{20}Mg_{19}Zn_{81}$), were reported. The crystal structures and prototypes of the five ternary compounds were determined as τ_1-*Immm* and La_3Al_{11}, τ_3-*Fm-3m* and $MnCu_2Al$, τ_4-*P6/mmm* and $TbCu_7$, τ_5-*P6*$_3$*/mmc* and $Sm_3Mg_{13}Zn_{30}$, and τ_7-*F-43m* and $Ce_{20}Mg_{19}Zn_{81}$. The crystal structures of $CeMg_{1-x}Zn_x$ continuous solid solution and of $CeMg_{12-x}Zn_x$ and $CeMg_{3-x}Zn_x$ limited solid solutions were determined precisely. In the work of Pavlyuk *et al*. [15], $Mg_{51}Zn_{20}$ was shown to be a stable phase equilibrating with (α-Mg), τ_2, $Mg_{12}Zn_{13}$ and $Ce(Mg,Zn)_{10.1}$ at

197 °C. However, $Mg_{51}Zn_{20}$ is only stable in the temperature range of 321–341 °C [16] and was not detected by other authors [9,13], who studied the system at higher temperatures.

Figure 1. Experimental Ce-Mg-Zn isothermal section studied by (**a**) Melnik *et al*. [9] at 300 °C; (**b**) Kevorkov and Pekguleryuz [13] at 350 °C; (**c**) Pavlyuk *et al*. [15] at 197 °C.

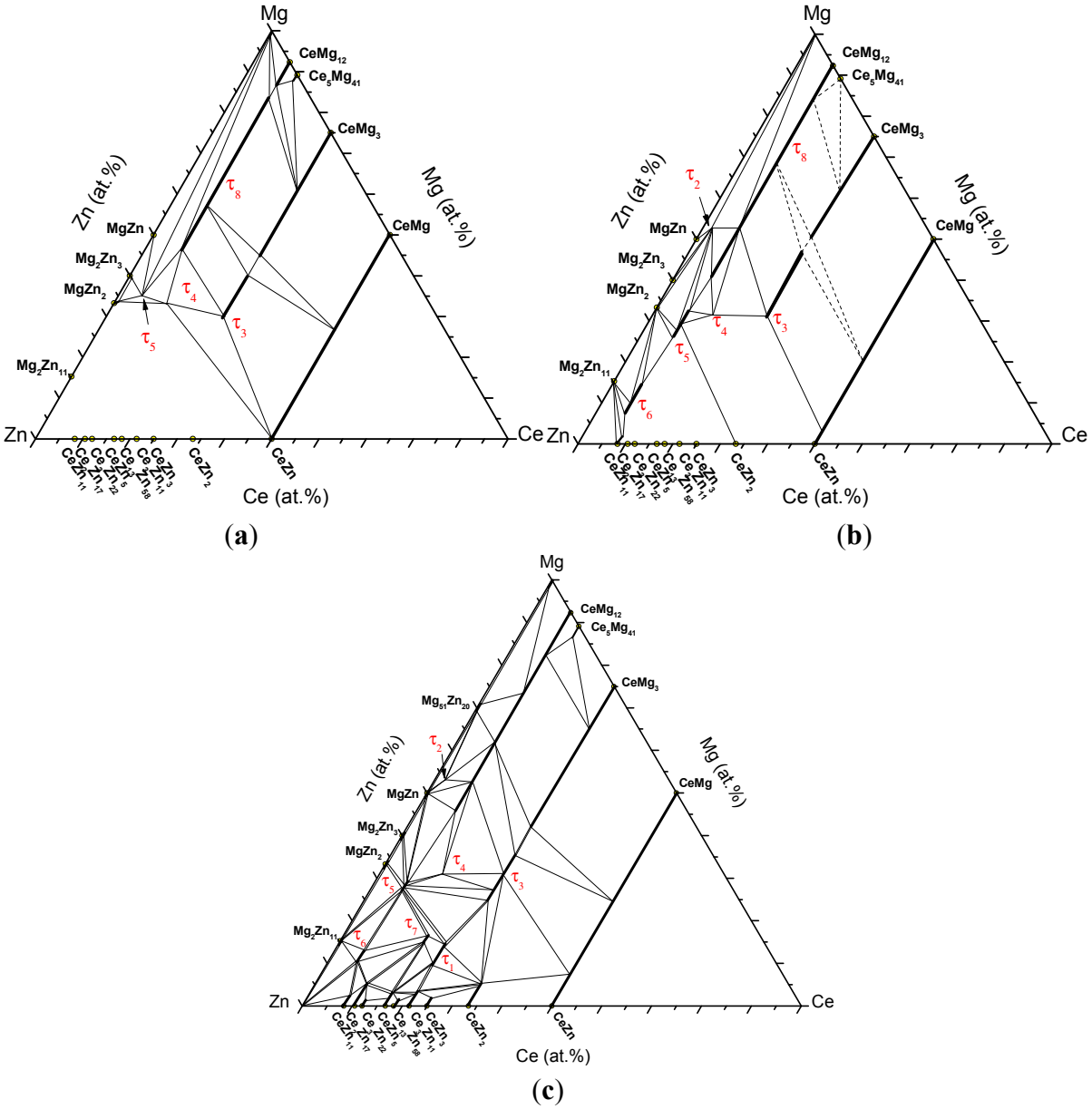

Table 1 summarizes the ternary phases in the Ce-Mg-Zn system at different temperatures, as reported in the literature [1,5,9,10,13–15]. The ternary compounds observed in the current work will be given the same naming system as reported by Pavlyuk *et al*. [15].

The lowest temperature liquid in the Ce-Mg-Zn was reported around 340 °C [11,14]. In order to avoid liquid phase formation, the current work was performed at 300 °C. The main objective of this work is to establish the Ce-Mg-Zn isothermal section in the full composition range at 300 °C experimentally by means of diffusion couples and key alloys, using XRD, SEM/WDS and metallography. This will help in resolving the inconsistent data of the literature and will give a better understanding of the phase relationships in the system, which is necessary for Mg-based alloy design and development.

Table 1. List of ternary phases in the Ce-Mg-Zn system reported in the literature.

	Phase	Reference					
		[1]	[5]	[9]	[10]	[13]	[15]
		350 °C	400 °C	300 °C		350 °C	197 °C
τ_1	$Ce_6Mg_3Zn_{19}$	-	-	-	-	-	$Ce_3(Zn_{0.863}Mg_{0.137})_{11}$
τ_2	$CeMg_{29}Zn_{25}$	-	-	-	-	Phase2	$CeMg_{29.2}Zn_{24.8}$
τ_3	$Ce_2Mg_3Zn_3$	-	-	$Ce_2Mg_3Zn_3$	-	Phase3	$CeMg_{1+x}Zn_{2-x}$ $0 \le x \le 0.48$
τ_4	$CeMg_{2.5}Zn_{4.5}$	-	-	$CeMg_3Zn_5$	-	Phase4	$CeMg_{2.5}Zn_{4.5}$
τ_5	$Ce_3Mg_{13}Zn_{30}$	-	-	$CeMg_7Zn_{12}$	$CeMg_7Zn_{12}$	Phase5	$Ce_3Mg_{13}Zn_{30}$
τ_6	$CeMg_{2.3-x}Zn_{12.8+x}$; $0 \le x \le 1.1$	-	-	-	-	Phase6	$CeMg_{2.3-1.2}Zn_{12.8-13.9}$
τ_7	$CeMgZn_4$	-	-	-	-	-	$Ce_{20}Mg_{19}Zn_{81}$
τ_8	$Ce(Mg_{1-z}Zn_y)_{11}$; $0.096 \le y \le 0.43$	$Ce(Mg_{1-y}Zn_y)_{11}$ $0.096 \le y \le 0.43$	$Ce(Mg_{1-y}Zn_y)_{11}$ $0.096 \le y \le 0.43$	$Ce(Mg,Zn)_{10.1}$	$Ce(Mg,Zn)_{10.1}$	Phase1	-

3. Results and Discussion

The diffusion couple technique combined with the selected equilibrated alloys was used to achieve more reliable information about the Ce-Mg-Zn isothermal section at 300 °C. This combination guarantees the accuracy of the obtained phase equilibrium information. The phase equilibria were determined by means of solid-solid diffusion couples and a diffusion multiple. In this work, the diffusion multiple and three diffusion couples will be presented along with the results of the key alloys.

Figure 2. (**a**,**b**) SEM micrographs of the Ce-Mg-Zn diffusion multiple annealed at 300 °C for 21 days. The end-members are given by the chemical symbols, and the diffusion layers are given by the numbers.

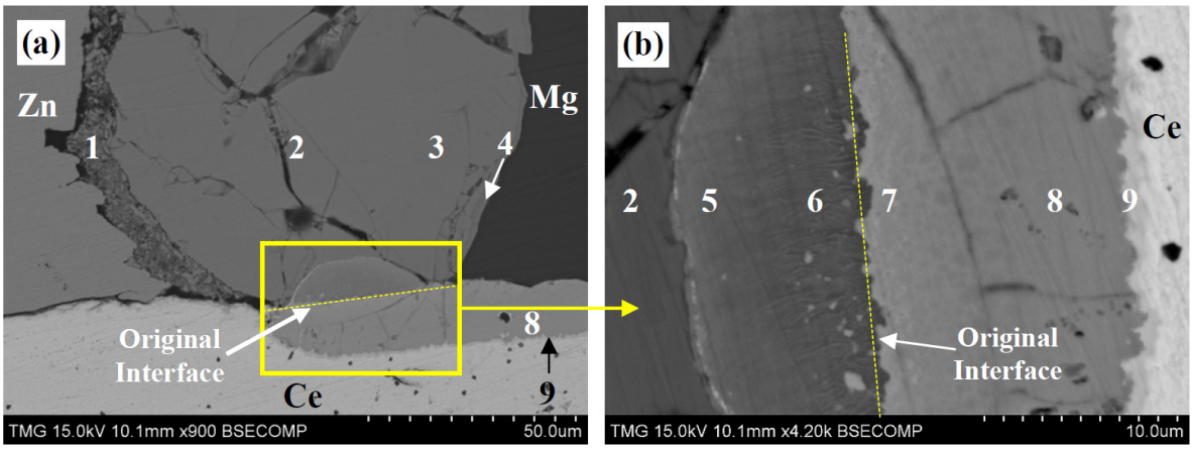

3.1. Diffusion Multiple

The end-members of the diffusion multiple were prepared from three pure metals (Ce, Mg and Zn). Initially, the interface of the Mg and Zn end-members was polished using a 1-μm diamond suspension; then, the two members were screwed together using a 4-mm bolt and nut. After that, the assembled Mg and Zn pieces were treated as one-unit and polished in the same way as described earlier to be attached

to the pure Ce member, using a stainless-steel clamping ring. The idea was to obtain multiple diffusion, in the reaction zone, between the binaries and the ternary mixing at the triple point. The micrograph of the diffusion multiple is presented in Figure 2a,b. Figure 2b is the diffusion zone, magnified and rotated 90° counter clock wise of Figure 2a.

From Figure 2, diffusion Zones 1, 2, 3 and 4 represent the diffusion in the Mg-Zn binary system. These diffusion zones were recognized as Mg_2Zn_{11}, $MgZn_2$, Mg_2Zn_3 and $Mg_{12}Zn_{13}$, respectively. Zones 8 and 9 belong to the Ce-Mg binary system, and their composition represents the $CeMg_3$ and CeMg binary compounds. No diffusion occurred between pure-Ce and pure-Zn at 300 °C after 21 days. Diffusion Zones 5, 6 and 7 represent ternary diffusion zones occurring from the reaction at the triple point. WDS spot analysis was performed for each individual zone. The WDS spot results are listed in Table 2.

Table 2. WDS spot analysis of the different diffusion zones of the diffusion multiple.

Zone	Composition (at.%)			Corresponding phase
	Ce	Mg	Zn	
Ce (end-member)	100	-	-	Ce
Mg (end-member)	-	100	-	Mg
Zn (end-member)	-	-	100	Zn
1	-	16.9	83.1	Mg_2Zn_{11}
2	-	32.9	67.1	$MgZn_2$
3	-	37.2	62.8	Mg_2Zn_3
4	-	43.5	56.5	$Mg_{12}Zn_{13}$
5	8.1	31.8	60.1	τ_5
6	9.5	55–67.1	35.5–23.3	τ_8
7	25	46.2–63.8	28.8–11.2	$Ce(Mg,Zn)_3$
8	25.5	74.5	-	$CeMg_3$
9	51.6	48.4	-	CeMg

The WDS line-scan was performed across the microstructure shown in Figure 2b (diffusion layers located between Zone 2 and pure Ce end-members). Figure 3 demonstrates the composition profile of the three elements along the WDS line-scan.

According to the profile shown in Figure 3, the ternary compound in Zone 6 and the solid solution in Zone 7 were characterized based on the substitution of Mg with Zn atoms. The composition of the three elements in Zone 6 matches with the composition of the ternary compound, $Ce(Mg_{1-y}Zn_y)_{11}$ ($0.33 \leq y \leq 0.45$ at.%), which is denoted as τ_8 in this work. Zone 7 represents the $Ce(Mg,Zn)_3$ ternary solid solution with 25 at.% Ce and 46.2–75.0 at.% Mg. It is worth mentioning that the solubility limits of Zones 6 and 7 are not accurate, since these were estimated from thin layers. However, the obtained data were enough to acquire the phase relations.

Figure 3. The WDS line-scan across diffusion layers located between Zone 2 and pure Ce end-member. The black-squared numbers given in the composition profile correspond to the number of diffusion zones indicated in Figure 2 and Table 2.

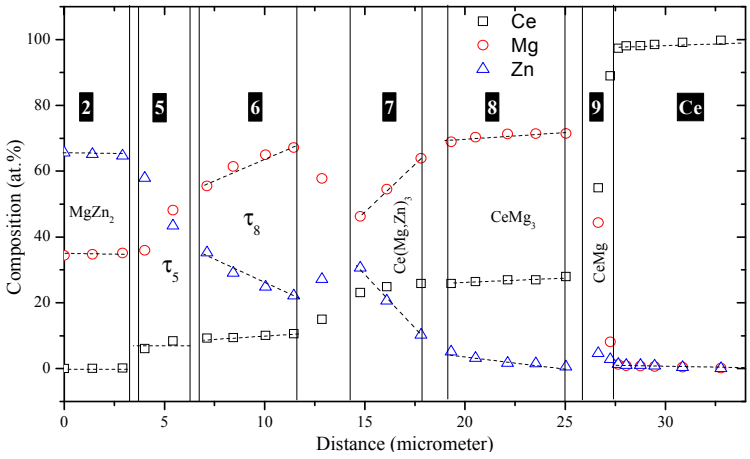

The composition of the ternary compound in Zone 5 was detected by WDS spot analysis as 8.1 at.% Ce, 31.8 at.% Mg and 60.1 at.% Zn. This composition matches with the composition of the $CeMg_7Zn_{12}$ ternary compound and given the symbol τ_5 in this work. The diffusion scenario between Zone 8 and pure Ce end-member represents a binary diffusion behavior, because no Zn was detected beyond the interface between Zones 8 and 9. This binary diffusion can be described as follows: $CeMg_3$ (Zone 8) → CeMg (Zone 9) → Ce (end-member).

Based on the microstructures of the diffusion zones and the WDS composition profile, the diffusion path was depicted as follows: $MgZn_2$ (Zone 2) → $Ce_3Mg_{13}Zn_{30}$ → $Ce(Mg,Zn)_{10.1}$ → $CeMg_3Zn_5$ → $CeMg_3$ → CeMg (Zone 9). The arrows used here represent the diffusion path and not a chemical reaction. The diffusion path depicted from diffusion multiple is represented graphically in Figure 4.

Figure 4. Diffusion path depicted from the diffusion multiple. Numbers in black boxes represent the diffusion zones indicated on the diffusion couple micrographs. Numbers on the right-hand side represent the phase equilibrium at every zone.

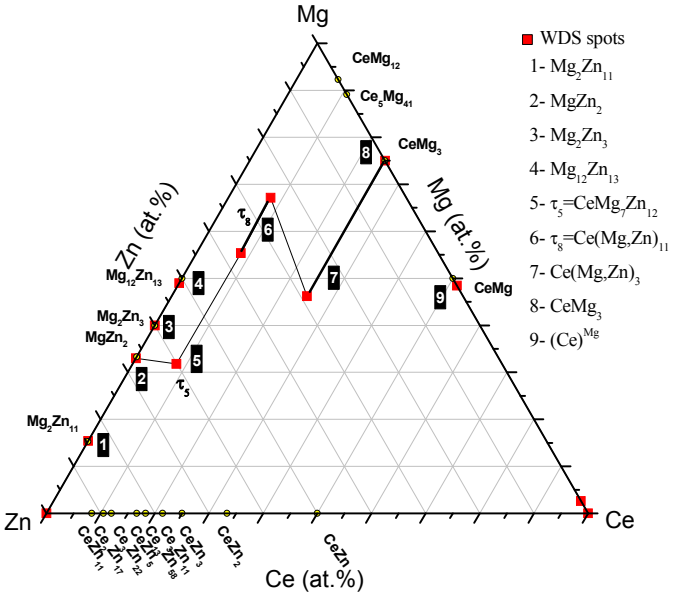

3.2. Diffusion Couples

3.2.1. Diffusion Couple 1: Zn/5.5 Ce-94.5 Mg at.%

The SEM micrograph of the solid-solid diffusion Couple 1 is presented in Figure 5a–c. The first end-member was made from pure Zn. The second end-member was made from an Mg and $CeMg_{12}$ two-phase binary alloy shown in Figure 5d. Diffusion Couple 1 showed very peculiar phase morphologies between the two end-members, indicating the difficulty of extracting the phase relationships from this couple. These morphologies, however, are rich with information about the phase relationships, which normally requires a large number of key alloys to be revealed. WDS spot analysis was carried out for every component of these diffusion zones. The WDS spot analysis results are listed in Table 3.

Figure 5. (**a**–**c**) SEM micrographs of diffusion Couple 1 annealed at 300 °C for 21 days; (**d**) SEM micrograph of the Mg + $CeMg_{12}$ two-phase alloy (end-member).

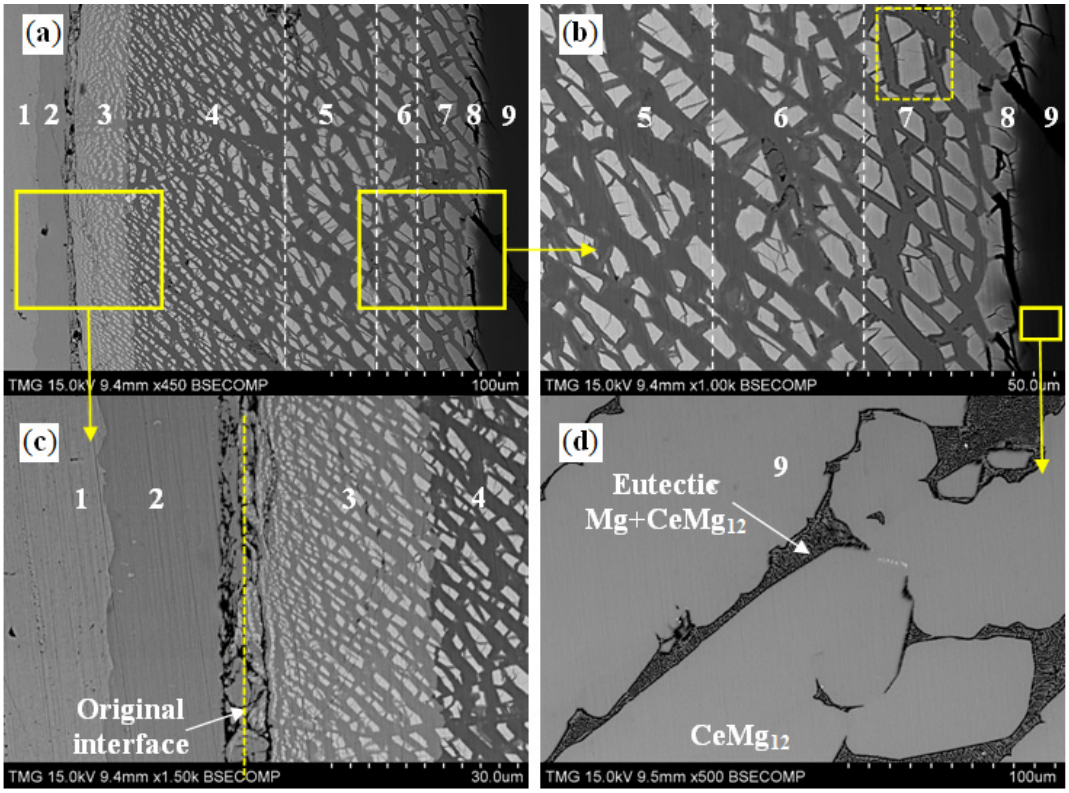

Upon annealing, nine diffusion zones formed. Diffusion Zone 2 represents the single phase of around 20 μm in width. Diffusion Zones 3–5 show layers with two phases. Diffusion Zones 6–8 show peritectic-like phase morphologies. Thus, Zones 6–8 contain two two-phase equilibria, *i.e.*, Solid A with Solid B and Solid B with Solid C, as illustrated in Zone 7 of Figure 5b and Table 3.

The SEM micrograph of diffusion Couple 1 in Figure 5a showed a white phase and islanding within diffusion Zones 3–8, and the grey phase is the matrix. WDS spots were performed across diffusion Zones 3–8 to measure the composition of the white phase islands and the grey phase in the matrix. Figure 6a,b shows the composition profile of the white and grey phases across the diffusion couple. The *x*-axis does not represent a metric distance; hence, it was labeled as a step, because these readings were taken across the diffusion zone with no exact spatial measurements.

Table 3. WDS spot analysis of different diffusion zones of diffusion Couple 1.

Zone	Composition (at.%)			Corresponding phase
	Ce	Mg	Zn	
1 (end-member)	-	-	100	Zn
2	-	15.6	84.4	Mg_2Zn_{11}
3	-	15.0	84.9	Mg_2Zn_{11} (grey)
	10.9	1.3	87.8	(Ce_2Zn_{17})
4	<1.0	32.8	67.1	$MgZn_2$ (grey)
	8.0	8.2	83.8	τ_6
5	-	33.4	66.6	$MgZn_2$ (grey)
	8.2	30.2	61.6	τ_5 (white)
6	7.9	36.0	56.1	τ_5 (white)
	0.1	32.8	67.1	$MgZn_2$ (grey)
	0.1	32.8	67.1	$MgZn_2$ (grey)
	2.3	49.0	48.7	τ_2
7	2.3	49.0	48.7	τ_2
	0.2	38.9	60.9	Mg_2Zn_3 (grey)
	8.6	42.4	49.0	τ_8 (white)
	2.3	49.0	48.7	τ_2
8	-	100	-	Mg
	2.3	49.0	48.7	τ_2
	8.1	53.2	38.7	τ_8 (white)
	-	100	-	Mg
9 (end-member)	8.66	91.34	-	$Ce(Mg,Zn)_{12}$
	-	100	-	Mg

Figure 6. The WDS composition profile of the (**a**) white phase islanding in the two-phase diffusion Zones 4–9; (**b**) the grey phase in the matrix of the same diffusion zones, including Zone 2.

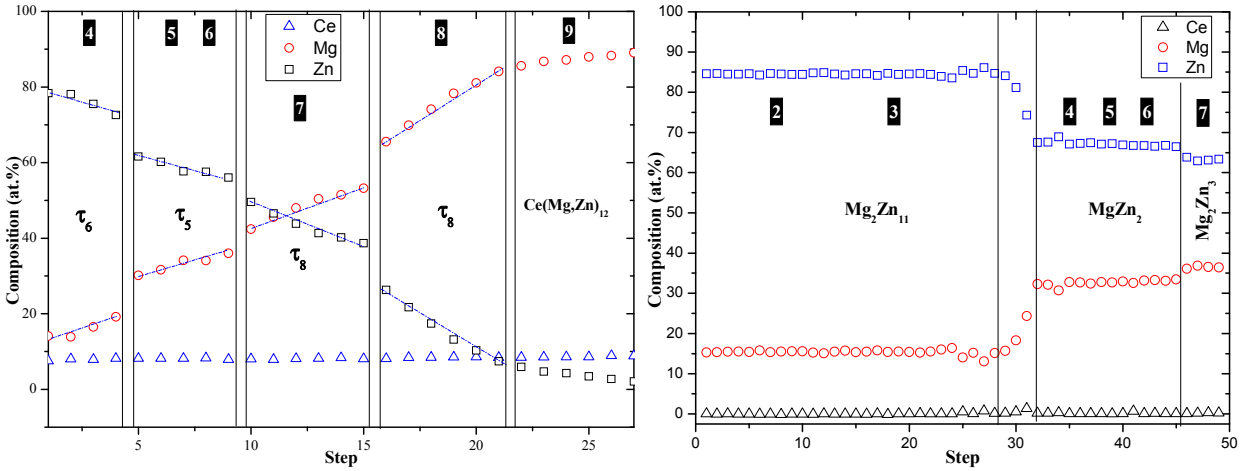

(**a**) (**b**)

One binary compound, $CeMg_{12}$, and three linear ternary compounds, τ_6 ($CeMg_{2.3-x}Zn_{12.8+x}$; $0 \leq x \leq 1.1$), τ_5 ($CeMg_7Zn_{12}$) and τ_8 ($Ce(Mg_{1-y}Zn_y)_{11}$; $0.096 \leq y \leq 0.43$), were detected from the white

phase profile in Figure 6a, whereas, three binary compounds (Mg_2Zn_{11}, $MgZn_2$ and Mg_2Zn_3) were detected in the grey phase profile (Figure 6b). The concentration of Ce was almost constant within the ternary phases' profile in Figure 6a.

The sequence of the phases in the grey phase matrix was similar to that of the Mg-Zn binary diffusion couple, annealed at 300 °C and 21 days, shown in Figure 7a. WDS spot results of the Mg-Zn diffusion couple are listed in Table 4. The ternary diffusion Couple 1 was compared with the Mg-Zn binary diffusion couple to give a better understanding of the phase relations between the Mg-Zn binary compounds and the τ_5, τ_6 and τ_8 ternary compounds. In other words, the ternary compounds were distributed in a matrix of Mg-Zn compound layers, as illustrated in Figure 7b.

Figure 7. (**a**) SEM micrograph of the Mg-Zn binary diffusion couple annealed at 300 °C for 21 days; (**b**) sketch of the ternary diffusion Couple 1 showing three ternary compounds islanding in the Mg-Zn compound layers.

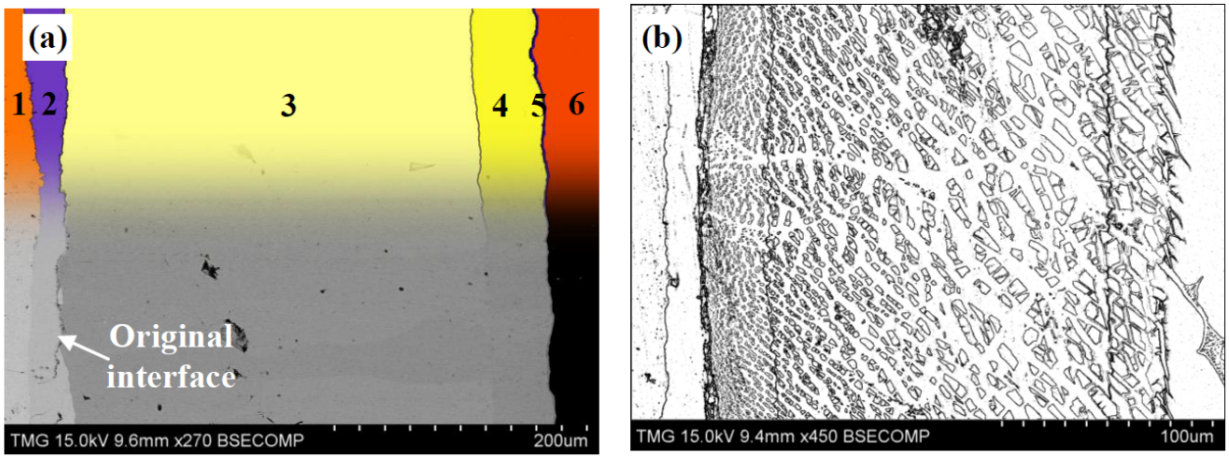

Table 4. WDS spot analysis of the Mg-Zn binary diffusion couple.

Zone	Composition (at.%)		Corresponding phase
	Mg	Zn	
1 (end-member)	-	100	Zn
2	15.3	84.7	Mg_2Zn_{11}
3	67.1	32.9	$MgZn_2$
4	61.8	39.2	Mg_2Zn_3
5	52.3	47.7	$Mg_{12}Zn_{13}$
6 (end-member)	100	-	Mg

EDS elemental mapping was used to define the composition of diffusion Zones 5 to 9, shown in Figure 8a. The Ce, Mg and Zn elemental maps are shown in Figure 8b–d, respectively. The color contrast of the Mg element, Figure 8c, revealed that the dark phase at the interface between Zones 8 and 9 is pure Mg and not a crack, as was suspected. The corresponding phase relationships determined from this part of the diffusion couple will be discussed in combination with Figure 9.

Figure 8. (**a**) SEM micrograph of Zones 5–8 of diffusion Couple 1; (**b**–**d**) EDS elemental maps of Ce, Mg and Zn, respectively.

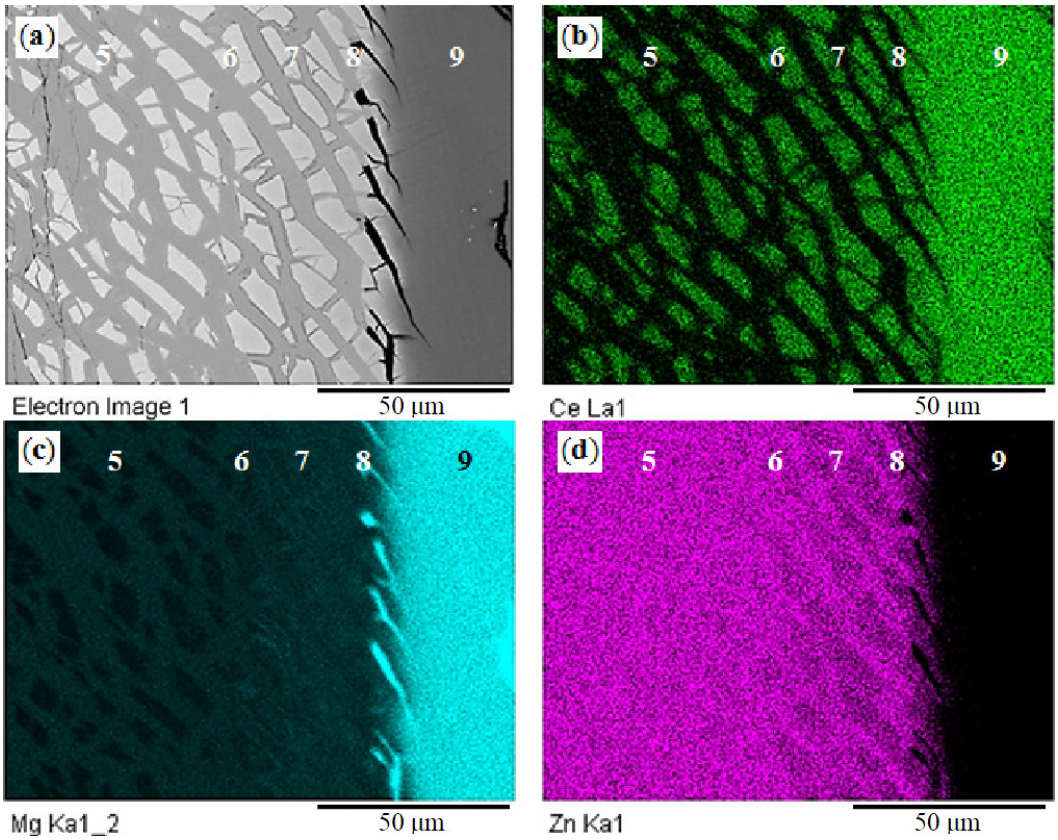

Figure 9. SEM micrograph of diffusion Zones 7 and 8 of diffusion Couple 1.

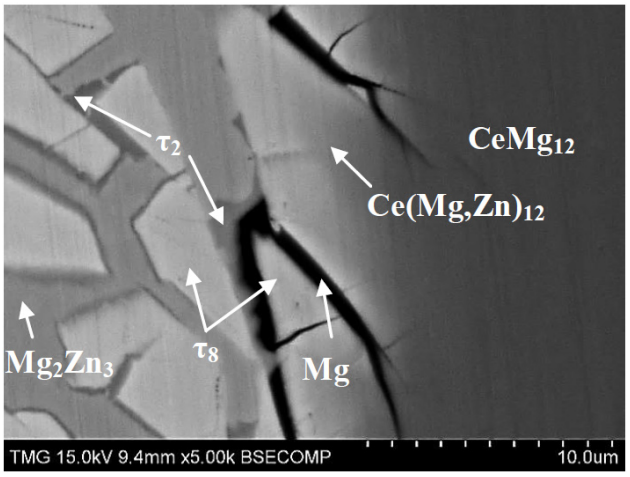

The SEM micrograph shown in Figure 9 shows the formation of a dark phase falling between τ_8 and pure Mg phases. This phase is in equilibrium with τ_8, Mg_2Zn_3, $MgZn_2$, τ_5 and pure Mg. WDS spot analysis revealed that this phase is τ_2 ($CeMg_{29.2}Zn_{24.8}$) according to Table 1. Based on its chemical composition, τ_2 is located near the binary $Mg_{12}Zn_{13}$. However, the binary $Mg_{12}Zn_{13}$ appears as a thin layer in Figure 7 (zone #5). It is expected that the $Mg_{12}Zn_{13}$ layer was breaking into smaller parts upon the subsequent formation of the two ternary compounds, τ_5 and τ_8, providing the 2.0 at.% Ce necessary to form τ_2.

One can raise an issue regarding the morphology of the scattered ternary compounds over a matrix of Mg-Zn compounds. It is presumed that the scattered formation of the ternary compounds was due to the preferential reaction of the diffusing species. Referring to the diffusion multiple in Figure 2a, the Mg-Zn binary diffusion couple has thicker diffusion layers than those of the Ce-Mg binary couple, as well as no diffusion occurred in the Ce-Zn binary diffusion couple at 300 °C and 21 days. In conclusion, the mobility of the atoms in the Mg-Zn system is higher than the atoms in both Ce-Mg and Ce-Zn systems. This conclusion will be discussed further below.

The composition of Ce was constant at 8.2 at.% in the profile of the $Ce(Mg,Zn)_{12}$ solid solution and the ternary compounds, τ_8, τ_5 and τ_6, shown in Figure 6a. However, the Ce concentration must be 7.6 at.% Ce for $Ce(Mg,Zn)_{12}$. This difference could be due to the error of the WDS measurements, which was estimated as ±1 at.% for Ce. Thus, it is most likely that the ternary compounds were formed from the $Ce(Mg,Zn)_{12}$ due to the Mg/Zn atomic exchange. This can also be supported by monitoring the end of the white phase traces, which can indicate the original location of the interface between the two end-members. Figure 5c shows clearly the location of the original interface where the crack exists, and the Mg_2Zn_{11} forms on both sides. The $Ce(Mg,Zn)_{12}$ solid solution is characterized by the substitution of Mg with Zn atoms. However, Zn has a smaller atomic radius (133 pm) than Mg (160 pm) [17]. Because of this difference in the atomic radii, distortion in the lattice structure might take place, and various ternary compounds with constant Ce concentration can be formed when Zn content reaches a threshold value. Evidence of this distortion, Figure 5a shows that the size of the white grains near the Zn-rich side is smaller than those adjacent to the $Ce(Mg,Zn)_{12}$ solid solution; this was also illustrated in Figure 7b. The grains with more Zn, due to substitution, show a smaller grain size. In addition, the substituted Mg atoms can be consumed by excess Zn atoms through the diffusion reaction to form Mg-Zn compounds. This can provide an explanation for the presence of pure-Mg (the black phase in Zones 8 and 9), which might be filtered from the solid solution due to the substitution mechanism.

In this system, the same phase morphology was observed in all diffusion couples containing Zn-rich end-members, specifically whenever a substitutional solid solution was encountered within the diffusion path. Diffusion Couple 2, for example, showed the same morphology, due to the Mg/Zn substitution in the $Ce(Mg,Zn)_3$ solid solution. The results of diffusion Couple 2 will be presented next.

According to the phase diagram rules, in a ternary system, the maximum number of phases in each diffusion layer is two. However, in diffusion Zones 6, 7 and 8, three phases were detected. These phases are $\tau_2 + \tau_5 + MgZn_2$, $\tau_5 + Mg_2Zn_3 + \tau_2$ and $\tau_8 + Mg_2Zn_3 + \tau_2$, respectively. This could be due to the anisotropic diffusion, which results sometimes during the sequential growth of the diffusion layers [18]. Such anisotropic growth might result in a volumetric mismatch, at the interface between two dissimilar phases, which occurs due to the lattice distortion. This can give more chance to the phases in the diffusion layers to break apart into scattered islands, equilibrating with the surrounding phases.

From the WDS spots and line-scans and the EDS elemental maps, the path of diffusion Couple 1 is represented graphically in Figure 10. The two end-members of diffusion Couple 1 are connected by a dashed line.

Figure 10. Phase equilibria depicted from the WDS spot analysis and line-scans across diffusion Couple 1. Numbers in black boxes represent the diffusion zones indicated on the diffusion couple micrographs. Numbers on the right-hand side represent the phases in every zone.

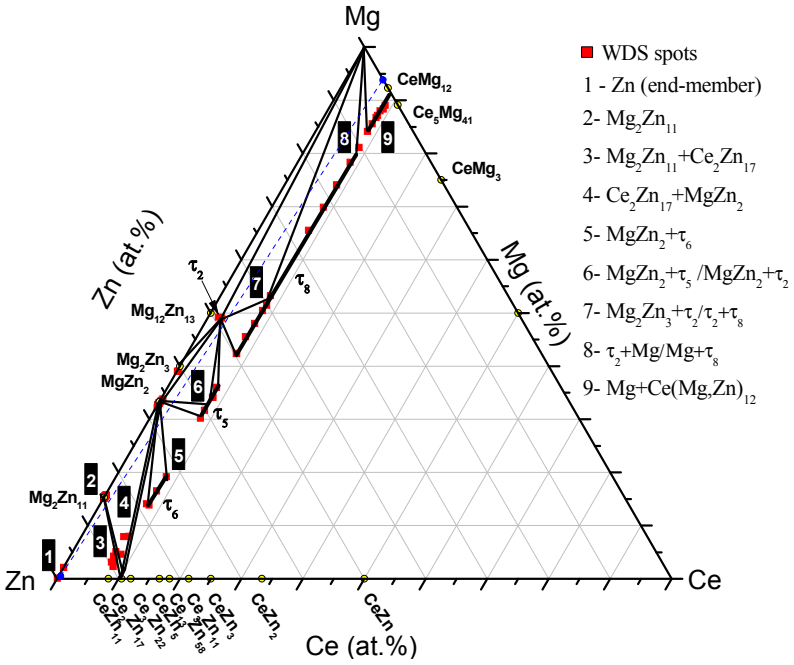

3.2.2. Diffusion Couple 2: Zn/27.0 Ce-73.0 Mg at.%

The SEM micrographs of the solid-solid diffusion Couple 2 are represented in Figure 11. The first end-member was made from pure Zn. The second end-member was made from the CeMg and $CeMg_3$ two-phase binary alloy. Diffusion Couple 2, similar to diffusion Couple 1, showed dispersed ternary compounds within a matrix of Mg-Zn binary compounds. Furthermore, the size of the white grains is decreasing with the increase in the Zn concentration. The occurrence of this morphology was thoroughly discussed within the results of diffusion Couple 1. In contrast to diffusion Couple 1, the results of diffusion Couple 2 showed that τ_3 is forming from the $Ce(Mg,Zn)_3$ solid solution due to the further substitution of Mg by Zn; then, τ_5 and τ_6 formed later, due to the increase in the Zn concentration.

Nine diffusion zones were determined and analyzed using WDS spot analysis and line-scans. Diffusion Zone 2 represents a single phase of 10 μm in thickness. Figure 11c is a magnified part from diffusion Couple 2 showing diffusion Zone 3, which represents a two-phase equilibrium between Mg_2Zn_{11} and Ce_2Zn_{17}. Diffusion Zones 4, 5, 6 and 7 have two compounds. The results of WDS spot analysis of diffusion Couple 2 are listed in Table 5. Figure 11b shows a very thin bright phase surrounding τ_3 ($Ce_2Mg_3Zn_3$), the white dendrites of Zone 7. Thus, the diffusion zone was magnified up to 10 kX (Figure 11d) to find out the composition of that phase using WDS spot analysis. The WDS spot analysis gave the following stoichiometry: 9.9 at.% Ce, 27.6 at.% Mg and 62.5 at.% Zn, which corresponding to τ_5 ($CeMg_7Zn_{12}$). This means that τ_5 is in equilibrium with $MgZn_2$ and τ_3. Furthermore, the composition profile is represented in the same figure to show the concentration gradient within τ_3, $Ce(Mg,Zn)_3$ and $CeMg_3$.

Figure 11. (**a**–**d**) SEM micrographs of diffusion Couple 2 annealed at 300 °C and 21 days.

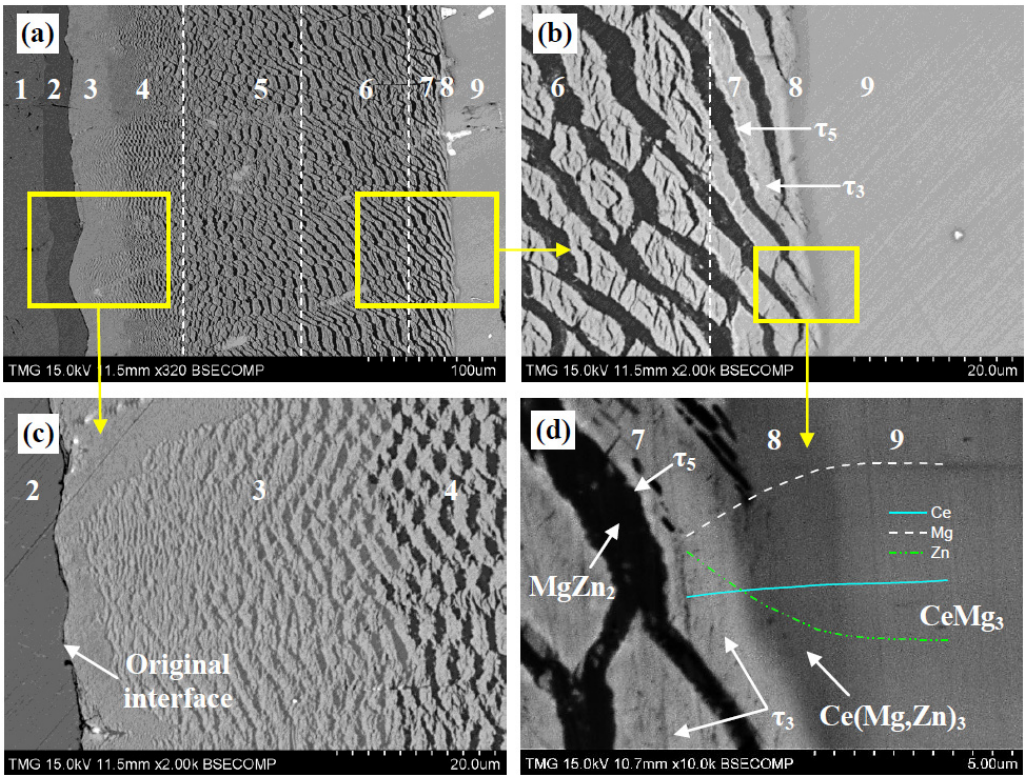

Table 5. WDS spot analysis of different diffusion zones of diffusion Couple 2.

Zone	Composition (at.%)			Corresponding phase
	Ce	Mg	Zn	
1 (end-member)	0	100	0	Zn
2	0	15.9	84.1	Mg_2Zn_{11}
3	7.2	2.9	89.9	(Ce_2Zn_{17})
	0	15.9	84.1	Mg_2Zn_{11}
4	7.5	5.2	87.3	(Ce_2Zn_{17})
	0.7	31.6	67.7	$MgZn_2$ (dark)
5	5.9	10.8	83.3	τ_6
	0.7	31.6	67.7	$MgZn_2$ (dark)
6	9.9	27.6	62.5	τ_5 (white)
	0.2	33.5	66.3	$MgZn_2$ (dark)
7	24.0	29.2	46.8	τ_3
	14.1	31.6	54.3	τ_5
8	24.3	57.8	17.9	$Ce(Mg,Zn)_3$
9 (end-member)	25.0	75.0	0	$CeMg_3$
	50.0	50.0	0	CeMg

Three ternary compounds, formed within the two-phase diffusion Zones 5 to 7, were observed. These compounds are τ_6, τ_5 and τ_3. The three compounds were characterized by the Mg/Zn substitution at a constant Ce concentration. The homogeneity ranges of these compounds were estimated, using WDS spot analysis, to be 6.0–12.4 at.% Mg, 24.0–31.6 at.% Mg and 25.0–29.0 at.% Mg, respectively.

Figure 12. (**a**) SEM micrograph of Zones 6, 7, 8 and 9 of diffusion Couple 2; (**b**–**d**) EDS elemental maps of Ce, Mg and Zn, respectively.

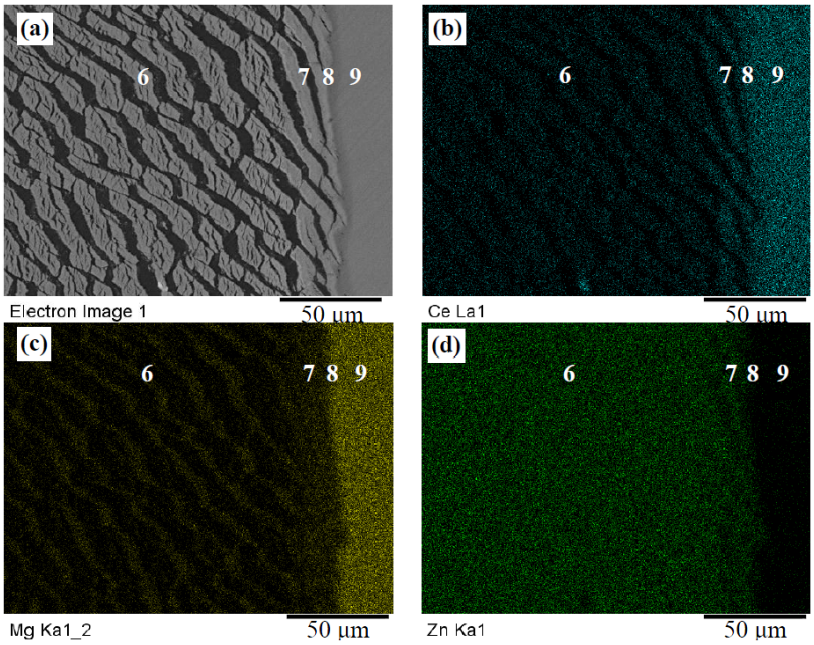

Figure 13. Phase equilibria depicted from the WDS spot analysis across diffusion Couple 2.

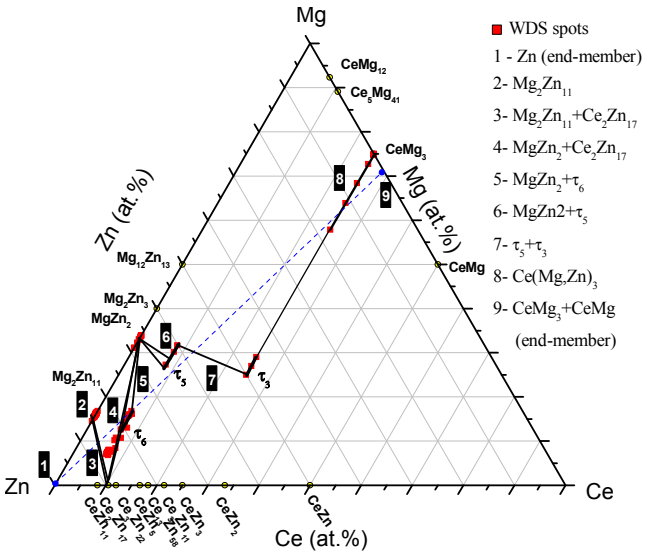

EDS elemental mapping was performed for diffusion Zones 6 to 9, as shown in Figure 12. The elemental maps were used to recognize the composition of every phase in the targeted area, as well as to determine the boundaries of every diffusion zone. Accordingly, the dark phase in the matrix of diffusion zones #6 and 7 (Figure 12a) was recognized to be a binary compound containing Mg and Zn, since the trace of this phase in the Ce map is dark. In contrast, the traces of the bright dendrites, for the same diffusion zones, represent ternary compounds. Figure 12b, shows that the ternary dendrites of Zone 7 contain higher Ce concentration in Zone 6, whereas, the proportion between Mg and Zn concentrations remains the same. However, these dendrites seem connected. The phase equilibria depicted from diffusion Couple 2 are represented graphically in Figure 13. The two end-members of diffusion Couple 2 are connected by a dashed line.

3.2.3. Diffusion Couple 3: Ce/97.0 Mg-3.0 Zn at.%

Solid-solid diffusion Couple 3, shown in Figure 14, was made from pure Ce and a binary alloy containing 83.0 at.% Mg and 17.0 at.% Zn (Figure 14b). Unlike other diffusion couples and the diffusion multiple, diffusion Couple 3 was annealed for 40 days instead of 21 days, since no diffusion layers were observed after 21 days of annealing. Thirty days was also tried, and no diffusion layers could be observed either. However, six diffusion layers with a total thickness of ~12 μm formed after 40 days of annealing. The WDS spot results of the diffusion zones are listed in Table 6. The WDS line-scan was performed across the diffusion zones of diffusion Couple 3. The composition of each layer was determined by, at least, two spots along the WDS line-scan, as shown in Figure 15.

Figure 14. (**a**), (**c**) and (**d**) SEM micrographs of diffusion Couple 3; (**b**) SEM micrograph of the 83 Mg-17 Zn (at.%) end-member.

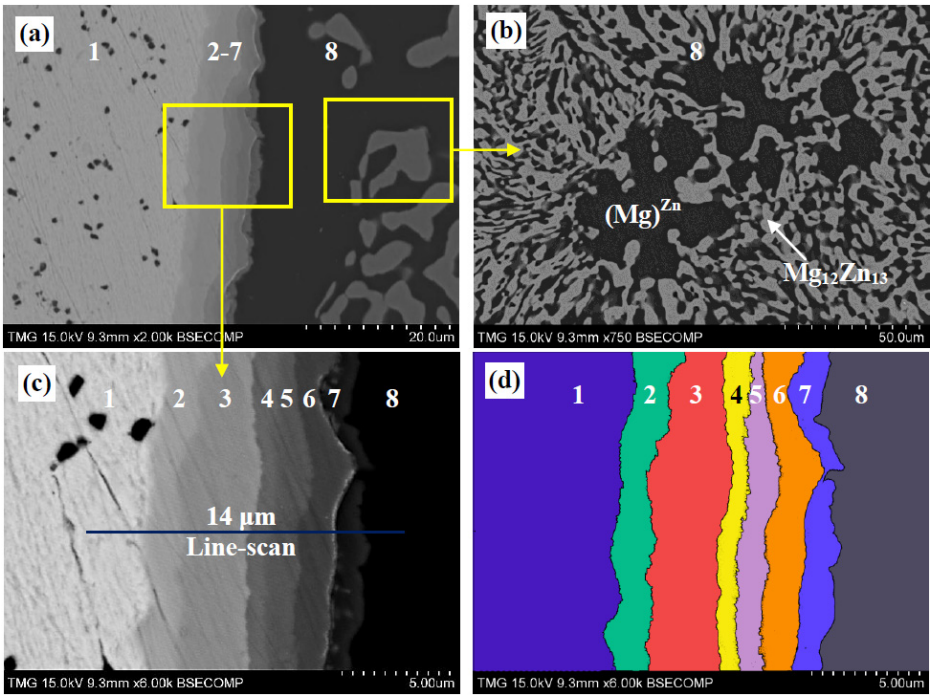

Table 6. WDS spot analysis of different diffusion zones of diffusion Couple 3.

Zone	Composition (at.%)			Corresponding phase
	Ce	Mg	Zn	
1 (end-member)	100	0	0	Ce
2	47.8	0	52.2	CeZn
3	32.1	0	67.9	$CeZn_2$
4	24.5	24.0	51.5	τ_3
5	16.7	20.4	62.9	τ_7
6	7.9	27.8	64.3	τ_5
7	2.0	53.7	44.3	τ_2
8 (end-member)	0	48.0	52.0	$Mg_{12}Zn_{13}$
	0	97.6	2.4	$(Mg)^{Zn}$

Figure 15. The WDS line-scan across diffusion Couple 3.

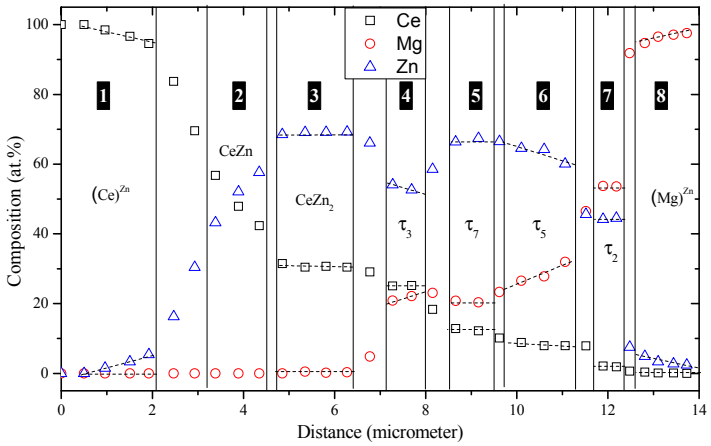

Based on the WDS spot analysis and line-scan, the solubility of Zn in Ce, Zone 1, was determined as 4.0 at.% Zn, as well as the solid solubility of Zn in Mg, Zone 8, was determined as 3.6 at.% Zn. Diffusion Zones 2 and 3 represent the CeZn and $CeZn_2$ binary compounds, respectively. Diffusion Zones 4 and 6 represent the ternary compounds, τ_3 and τ_5, which are characterised by the Mg/Zn substitution at a constant Ce composition. Diffusion Zones 5 and 7 represent the stoichiometric ternary compounds, τ_7 and τ_2, respectively.

According to WDS spot analysis and line-scans, the diffusion path of diffusion Couple 3 can be represented as follows: Pure Ce (end-member) → $(Ce)^{Zn}$ → CeZn → $CeZn_2$ → τ_3 → τ_7 → τ_5 → τ_2 → $(Mg)^{Zn}$ → $(Mg)^{Zn}$ + $Mg_{12}Zn_{13}$ (end-member). The diffusion path is represented graphically in Figure 16. The two end-members are connected by a dashed line.

Figure 16. Diffusion path depicted from diffusion Couple 3.

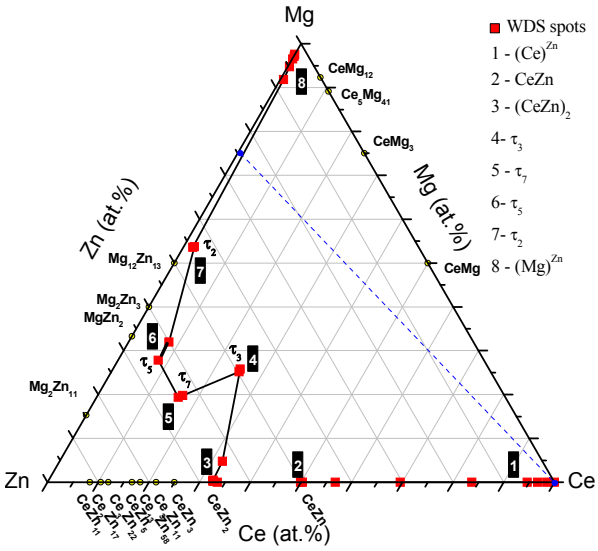

The diffusion path of diffusion Couple 3 (Figure 16) shows some of the phases, corresponding to the diffusion Zones 2–6 (Figure 14), that form near the Zn-rich side. In order to understand the diffusion reaction, the mass balance principle must be taken into account. In this case, the diffusion reaction can be described as follows: the pure Ce existing in the end-member of diffusion Couple 3 was diffusing against Mg and Zn atoms, which were provided by the two-phase alloy of the other end-

member. The atomic exchange took place, and the Ce concentration dropped gradually across the formed diffusion zones, as shown in the WDS composition profile in Figure 15. Accordingly, several Zn-rich ternary compounds were formed to the left side of the line connecting the two end-members. In this case, the mass of the reacted Ce and Zn must to be compensated with more Mg. Thus, the diffusion reaction switched its path sharply towards the Mg-rich corner after Zone 5, and the two-phase end-member contributed to this compensation by forming a considerably thick layer of Mg-rich solid solution, $(Mg)^{Zn}$ in Zone 8, to balance the mass. Therefore, the diffusion path fulfilled the mass balance condition by intersecting the line connecting the two end-members at least once.

Seven ternary compounds were detected in diffusion multiple and diffusion Couples 1, 2 and 3; these phases are τ_2, τ_3, τ_4, τ_5, τ_6, τ_7 and τ_8. Obviously, several of these compounds were observed in more than one couple, providing the confirmation of their presence in the system at 300 °C.

The three diffusion couples gave a clear idea about the phase equilibria in the Zn-rich corner, up to 33 at.% Mg and 10 at.% Ce; since their results in that part were consistent. Other regions of the Ce-Mg-Zn isothermal section at 300 °C were determined by the key alloy experiments, and their results are discussed in the following section.

3.3. Key Alloys Analysis

Key alloys were used to verify the results obtained from diffusion couples experiments and to cover the remaining parts of the Ce-Mg-Zn isothermal section at 300 °C. Thus, twenty eight key alloys were prepared with different compositions. The actual composition was obtained by the average of three EDS area-analysis. The actual composition of a few samples (1, 2, 4, 13 and 14), selected randomly, was measured using inductively coupled plasma-optical emission spectrometry (ICP-OEM) to confirm the EDS area measurements. Both EDS and ICP-OEM measurements were in good agreement. Figure 17 shows the actual composition obtained from the EDS and ICO-OEM methods.

Figure 17. The actual composition of the key alloys obtained by EDS area analysis and ICP-OEM.

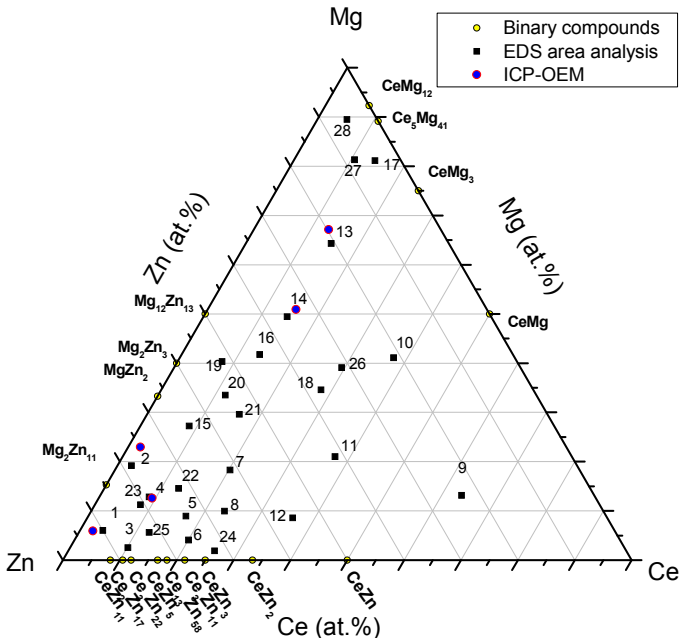

Alloys were brought to equilibrium after annealing at 300 °C for 30 days. WDS spot analysis was performed on the annealed samples to determine the composition of the observed phases. X-ray diffraction of the samples' was performed to identify the equilibrated phases and to verify the phase relations obtained from WDS analysis.

Table 7. WDS spot analysis of samples with three-phase equilibria.

Sample number	Actual composition EDS (at.%)			WDS composition (at.%)			Corresponding phase
	Ce	Mg	Zn	Ce	Mg	Zn	
1	4.0	6.0	90.0	10.4	0.8	88.8	(Ce_2Zn_{17})
				0.0	15.8	84.2	Mg_2Zn_{11}
				0.0	1.0	99.0	$(Zn)^{Mg}$
2	2.5	19.2	78.3	10.4	1.2	88.4	(Ce_2Zn_{17})
				0.0	15.1	84.9	Mg_2Zn_{11}
				0.0	33.1	66.9	$MgZn_2$
5	17.2	8.9	73.8	16.4	16.6	67.0	τ_7
				16.5	4.1	79.4	$(CeZn_5)$
				20.1	8.7	71.2	τ_1
7	20.2	18.3	61.5	16.3	16.7	67.0	τ_7
				24.5	23.3	52.2	τ_3
				20.6	8.6	70.8	τ_1
8	23.4	9.9	66.7	32.4	0.5	67.1	$(CeZn_2)$
				20.8	7.2	72.0	τ_1
				25.0	22.0	53.0	$Ce_2Mg_3Zn_3$
12	36.1	8.6	55.3	50.0	8.5	41.5	Ce(Mg,Zn)
				33.3	1.9	64.8	$(CeZn_2)$
				25.0	25.0	50.0	τ_3
16	13.7	41.7	44.6	25	25	50	τ_3
				14.3	28.9	56.8	τ_4
				8.5	56.8	34.7	τ_8
17	15.3	81.2	3.5	25.0	69.5	5.5	$Ce(Mg,Zn)_3$
				10.8	89.2	0	Ce_5Mg_{41}
				8.3	88.9	2.8	$Ce(Mg,Zn)_{12}$
24	25.7	1.6	72.7	32.0	0	68.0	$CeZn_2$
				20.5	2.6	76.9	(Ce_3Zn_{11})
				20.4	7.5	72.1	τ_1
25	12.3	5.6	82.1	16.3	4.5	79.2	$CeZn_5$
				11.2	2.2	86.6	(Ce_2Zn_{17})
				11.2	13.9	74.9	τ_6
28	5.2	89.5	5.3	8.6	79	12.4	τ_8
				8.6	85.3	6.1	$Ce(Mg,Zn)_{12}$
				1.0	97.5	1.5	$(Mg)^{Ce,Zn}$

3.3.1. Alloys with Three-Phase Equilibria

Several three-phase regions in the Ce-Mg-Zn isothermal section at 300 °C were determined by key alloys experiments. WDS spot analyses of samples with three-phase equilibria are listed in Table 7.

Figure 18 shows the SEM micrographs of some selected alloys with three-phase equilibria with the labels of the detected phases. X-ray powder diffraction patterns of Samples 1, 2 and 12, shown in Figure 19, are given as examples of the phase identification using X-ray diffraction analysis. However, XRD was performed on the all prepared samples. The results of WDS spot analysis and XRD were consistent for the phases of known crystal structures. More studies regarding the phases on the unknown crystal structures are still needed.

Figure 18. SEM micrographs of some samples of three-phase equilibria (**a**) Sample 1; (**b**) Sample 2; (**c**) Sample 8; (**d**) Sample 12; (**e**) Sample 16; (**f**) Sample 17.

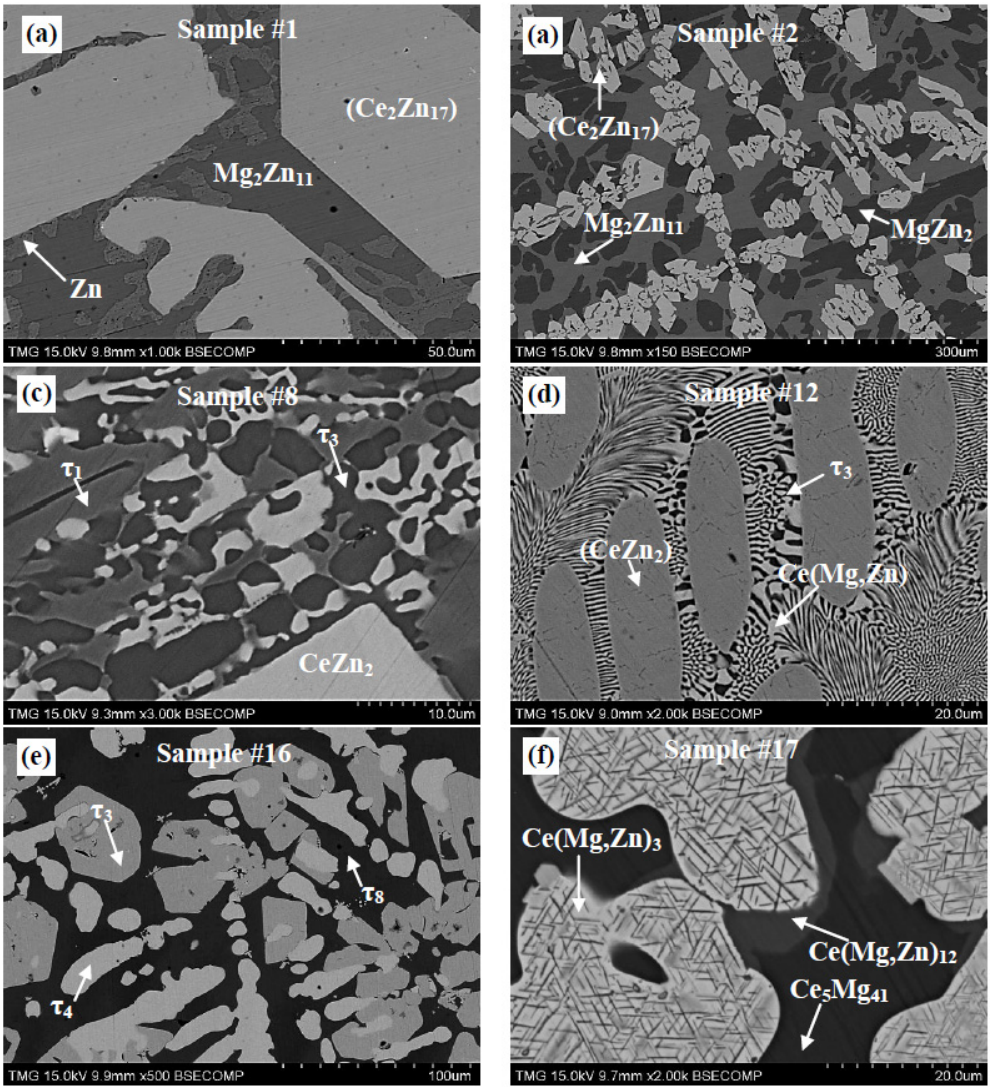

It is worth noting that Figure 18f exhibits a lamellar structure in the white grains. This structure has similarity to the so-called Widmanstätten pattern, which forms due to the lamellar growth of one phase in the crystal lattice of another phase [17]. Because these phases are very small, it was difficult to determine their composition by WDS spot analysis. However, using XRD analysis, $Ce(Mg,Zn)_{12}$, Ce_5Mg_{41} and $Ce(Mg,Zn)_3$ were positively determined in the diffraction pattern of Sample 17. Since $Ce(Mg,Zn)_{12}$ and Ce_5Mg_{41} are well identified according to WDS measurements, the white phase containing the lamellar structure is assigned as $Ce(Mg,Zn)_3$. The maximum solubility of Zn in $Ce(Mg,Zn)_3$ was found to be 5.5 at.% Zn.

Figure 19. The X-ray powder diffraction of the annealed Samples 1, 2 and 12 showing three phase equilibria. Silicon was used as a calibration standard to correct the zero shift and specimen displacement errors.

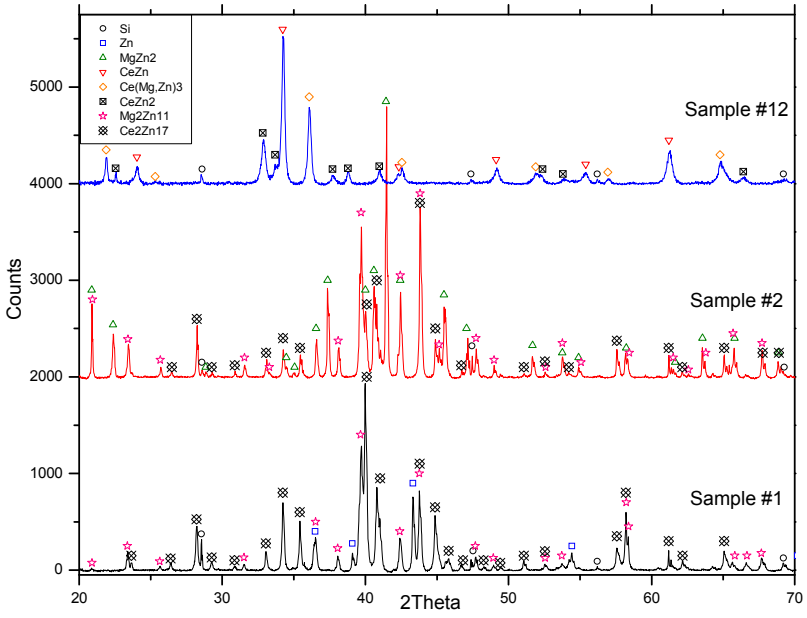

Figure 20. SEM micrographs of (**a**) Sample 3; (**b**) Sample 6; (**c**) Sample 9; (**d**) Sample 10; (**e**) Sample 14; (**f**) Sample 18.

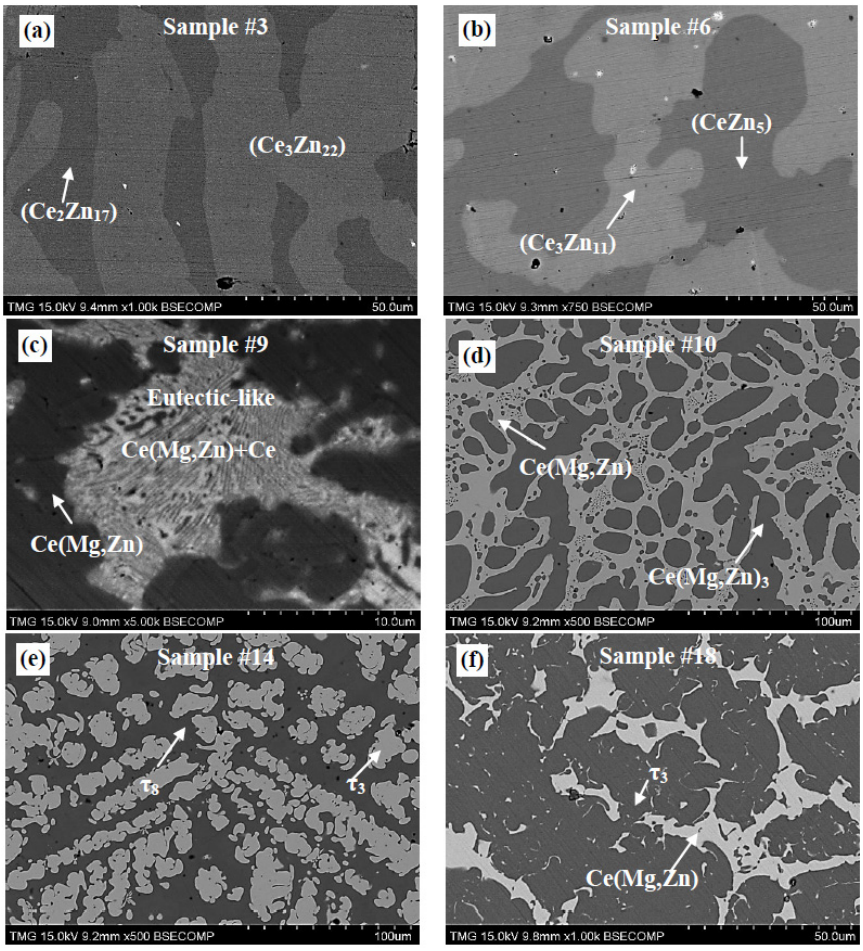

3.3.2. Alloys with Two-Phase Equilibria

Many two-phase regions, in the Ce-Mg-Zn isothermal section at 300 °C, were determined. In this section, selected alloys with two-phase equilibrium are presented Figure 20. The WDS spot analyses of samples with two-phase equilibria are listed in Table 8. The XRD patterns of Samples 3, 10 and 23, shown in Figure 21, are given as examples of the phase identification using X-ray diffraction analysis.

Table 8. WDS spot analysis of samples with two-phase equilibria.

Sample number	Actual composition EDS (at.%)			WDS composition (at.%)			Corresponding phase
	Ce	Mg	Zn	Ce	Mg	Zn	
3	10.1	2.5	87.4	11.9	1.1	87.0	(Ce_3Zn_{22})
				10.5	1.3	88.2	(Ce_2Zn_{17})
4	9.8	12.8	77.4	10.7	7.2	82.1	τ_6
				8.6	31.4	60.0	τ_5
6	20.0	4.1	75.9	20.8	2.1	77.1	Ce_3Zn_{11}
				18.1	3.5	78.4	($CeZn_5$)
9	63.5	13.1	23.4	100.0	0	0	Ce
				50.0	21.0	29	Ce(Mg,Zn)
10	37.6	71.0	31.4	25	55	20	Ce(Mg,Zn)
				50	24	26	$Ce(Mg,Zn)_3$
11	37.4	21.0	41.6	50	9	41	τ_3
				25	35.2	39.8	Ce(Mg,Zn)
13	15.1	63.3	20.6	25	47	28	$Ce(Mg,Zn)_3$
				7.8	77.6	14.6	τ_8
14	14.7	49.5	35.8	25	29.5	45.5	τ_3
				8.2	65.5	26.3	τ_8
15	10.1	25.3	64.6	8.8	41.2	50.0	τ_5
				10.5	10.8	78.7	τ_6
18	28.1	34.5	37.4	50	10	40	Ce(Mg,Zn)
				25	38	37	τ_3
19	9.2	41.3	49.5	10.1	20.8	69.1	τ_6
				7.3	41.5	51.2	τ_5
20	12.8	33.5	53.7	14.3	28.9	56.8	τ_4
				8.1	44.8	47.1	τ_5
23	8.1	11.2	80.7	10.5	3.6	85.9	(Ce_2Zn_{17})
				0	33.4	66.6	$MgZn_2$

The SEM micrograph of Sample 3, shown in Figure 20a, represents the two-phase equilibria between the two extended solid solutions from (Ce_2Zn_{17}) and (Ce_3Zn_{22}). Figure 20b represents the two ternary solid solutions ($Ce_{13}Zn_{58}$) and (Ce_3Zn_{11}) occurring in Sample 6. The maximum solubility of Mg in Ce-Zn binary compounds is listed in Table 8. High magnification was required to observe the phase relationships of Sample 9. Thus, the SEM micrograph of Sample 9 was magnified up to 5 kX, as shown in Figure 20c. A fine eutectic-like structure, containing Ce + Ce(Mg,Zn), was in equilibrium with the Ce(Mg,Zn) ternary solid solution. Other micrographs correspond to the phase equilibrium that can be inferred from the labels.

Based on the WDS and XRD analyses, the determined phases from the equilibrated key alloys are shown graphically in Figure 22. The key alloys with the actual composition are shown as bold circles. The arrows indicate the phase equilibria determined from the WDS and XRD studies of each alloy.

Figure 21. The X-ray powder diffraction of the annealed Samples 3, 10 and 23. Silicon was used as a calibration standard to correct the zero shift and specimen displacement errors.

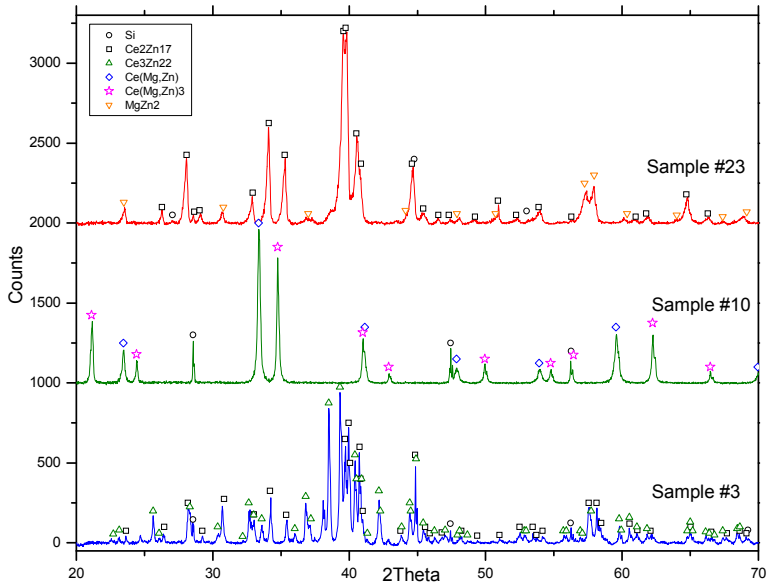

Figure 22. Phase relationships of the Ce-Mg-Zn isothermal section at 300 °C obtained from key alloy experiments.

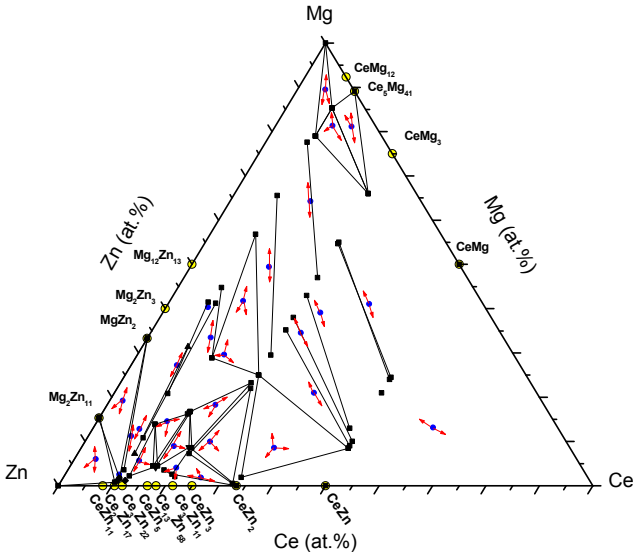

In addition to the seven ternary compounds observed by diffusion couples experiments, one ternary compound was detected by the key alloys experiments. This compound is τ_1 ($Ce_6Mg_3Zn_{19}$).

3.4. Ce-Mg-Zn Isothermal Section at 300 °C

The Ce-Mg-Zn isothermal section at 300 °C, constructed based on diffusion multiple/couples and equilibrated key alloy studies, is shown in Figure 23. Eight ternary compounds were found

and named τ_1 to τ_8. The system shows the ternary compounds and the solid solutions with wide homogeneity ranges.

Because of many wide two-phase fields, the determination of the boundary tie-lines needs a lot of key alloys to verify the phase equilibrium. In this work, however, tie-lines were interpolated based on the mass balance principle [6]. In this method, at least three tie-lines must be determined experimentally for each two-phase field. Two lines, parallel to the boundary composition lines, are extended from the two ends of each experimental tie-line until they intersect. Three intersection points are determined. Matching these points gives the balance curve, which represents the amount of the equilibrated phases *versus* composition. Each point on the curve represents an intersection of any tie-line that occurs in that field. Once the curve is determined, the process can be reversed, and additional tie-lines can be interpolated by extending two lines parallel to the phase boundary composition lines. Using the tie-line interpolation method, many regions in the Ce-Mg-Zn isothermal section could be determined, specifically the two three-phase regions, $\tau_8 + \tau_3 + Ce(Mg,Zn)_3$ and $\tau_3 + Ce(Mg,Zn)_3 + Ce(Mg,Zn)$.

Figure 23. The Ce-Mg-Zn isothermal section at 300 °C.

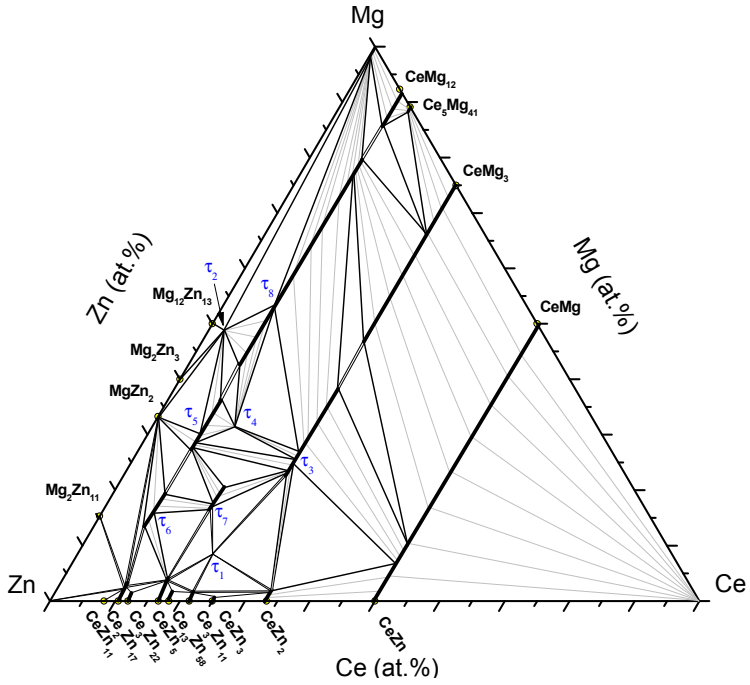

The ternary solubility of Zn in the Ce-Mg compounds was found to increase with decreasing Mg concentration. The same was observed by [9], whereas no solubility trend was reported by [13] and [15]. In this work, the ternary solid solubility of Zn in $CeMg_{12}$ and $CeMg_3$ was measured at 300 °C as 5.6 and 28.4 at.% Zn, respectively. These are in good agreement with the solubilities reported by [9] at the same annealing temperature. Furthermore, a complete solubility between CeMg and CeZn compounds was reported by [9,13,15] at different annealing temperatures. In this work, the complete solid solubility was confirmed experimentally using a diffusion couple made from alloys of these compounds, as shown in Figure 24a. This diffusion couple was annealed at 300 °C for 40 days. The composition profile obtained by the WDS line-scan is shown in Figure 24b. The composition profile shows the exchange of Mg and Zn around the interface (from left to right), whereas the concentration of Ce is constant.

Figure 24. (**a**) The SEM micrograph of the CeMg/CeZn diffusion couple annealed at 300 °C for 40 days; (**b**) the composition profile obtained by the WDS line-scan.

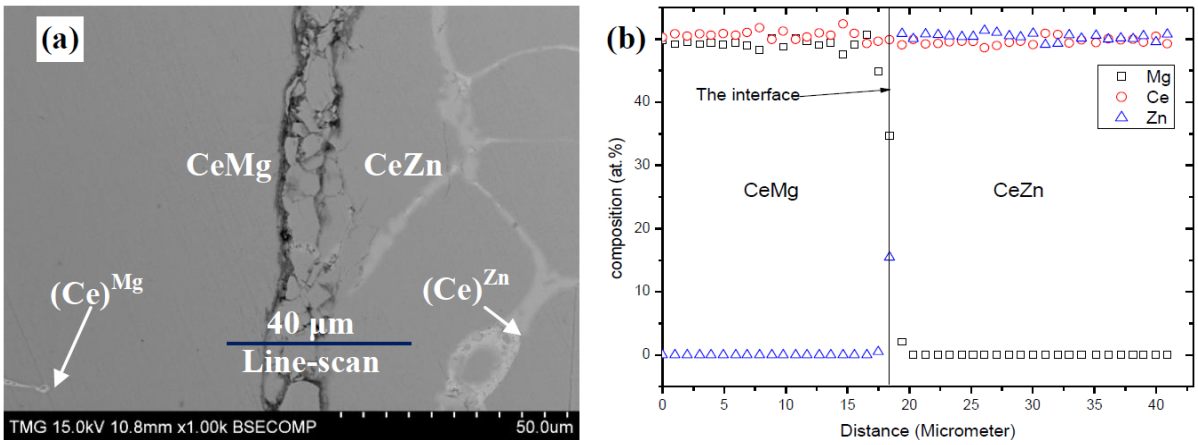

The Zn-rich side showed very complex phase relationships due to the existence of many ternary compounds. However, it was not possible to compare the current results with the available data of Melnik *et al.* [9] at 300 °C, because they did not establish the phase relations between all the compounds in this region. Furthermore, the phase relations in the same region were different than those in [13] and [15], due to the different annealing temperatures. Nevertheless, in the results obtained in the current work were verified using diffusion multiple/couples and equilibrated key alloys. The Mg-rich side showed relatively less complexity, since the $(Mg)^{Ce,Zn}$ ternary solid solution forms wide two-phase fields with τ_8 and $Ce(Mg,Zn)_{12}$. In this work, $Mg_{12}Zn_{13}$, τ_2, τ_8, $Ce(Mg,Zn)_{12}$ and $CeMg_{12}$ were found in equilibrium with $(Mg)^{Zn}$. This is similar to the results of Melnik *et al.* [9] to some extent, except that they reported equilibrium with τ_5 instead of τ_2. The Ce-rich side shows the simplest phase relations, because Ce is equilibrating with the complete solid solution Ce(Mg,Zn).

4. Experimental Procedure

In order to study the phase relationships in the Ce-Mg-Zn isothermal section at 300 °C, solid-solid diffusion couples along with key alloys were prepared and analyzed using a Hitachi (Tokyo, Japan) S-3400N SEM equipped with Oxford® (Abingdon, UK) EDS/WDS detectors and a PANalytical (Almelo, The Netherlands) X-ray diffractometer (Cu K-α radiations). EDS and WDS analysis were used to determine the phases and to quantify their compositions. Pure metals (Ce, Mg and Zn) were used as standards for WDS calibration. X-ray scans were performed on powder-form samples, in the range from 20 to 120 degree 2θ with a 0.02° step size, to identify and confirm the phases obtained by WDS measurements, since the stoichiometry of the Zn-rich compounds falls within the WDS error of measurements. X-ray phase analysis was carried out using X'pert Highscore Plus software [19]. The standard intensity data were taken from Pearson's Crystal Database [20]. Silicon was used in the powder samples as a calibration standard to correct the zero shift and specimen displacement.

4.1. Key Alloys Preparation

Pure elements were used for the preparation of key samples and diffusion couple end-members. Ce and Zn ingots with a purity of 99.9% and 99.99%, respectively, were supplied by Alfa Aesar Co.

(Haverhill, MA, USA) Mg ingots with a purity of 99.8% were supplied by CANMET Materials Technology Laboratory (Ottawa, ON, Canada). The key alloys were prepared in an electric-induction furnace with a tantalum crucible and argon atmosphere. It was difficult to prepare the Zn-rich alloys (75–92 at.% Zn) by melting the three pure metals together. A severe exothermal reaction between liquid Zn and solid Ce took place, and the material evaporated as a result. Because of this difficulty, Pavlyuk *et al*. [15] prepared the Ce-rich (>50 at.%) samples by sintering the metal powders followed by arc-melting in argon atmosphere, whereas the Mg-rich and Zn-rich samples were prepared in sealed Ta crucibles.

Alloys near the Zn-rich corner were prepared by adding pure Zn to Ce-Mg alloys; whereas other compositions were prepared by melting the three pure metals. Excess amounts of Mg and Zn (around 10%) were added to compensate for losses due to evaporation. The alloys were melted several times to ensure the composition homogeneity. The actual global composition was determined using Ultima (Longjumeau, France) optical emission spectrometer (OEM)-inductively coupled plasma (ICP). ICP standards of pure metals, 1000 mg/L in HNO_3, were supplied by Fischer Scientific Co. (Waltham, MA, USA) The average of three readings, at least, was considered as the global composition of the alloy. EDS/SEM area analysis was also performed to obtain the actual composition prediction; because the samples structure was homogeneous. Both ICP and EDS results were in good agreement.

4.2. Solid-Solid Diffusion Couples

The end-members of the solid-solid diffusion couples were prepared from pure metals and/or alloys. The contacting surfaces were ground gradually up to 1200 grit SiC paper using 99% pure ethanol as a lubricant and to prevent oxidation. High friction between samples and SiC papers was avoided to eliminate sparking during grinding due to Ce. After that, the ground surfaces were polished down to 1 μm using an alcohol diamond suspension. The end-members were strongly tightened together using stainless steel clamping rings.

For annealing purposes, samples and diffusion couples were wrapped in tantalum foil and encapsulated inside an argon-purged quartz tube with an inside pressure of about 8×10^{-1} torr. To reach equilibrium, diffusion couples and key alloys were heated up to 300 °C for a predefined period of time. The annealing time was chosen as 21 days based on the composition of the selected end-members. Furthermore, visual observation of the annealing tubes was used to stop the annealing process when the quartz tube became dark, indicating significant evaporation. After annealing, the quartz tubes, containing samples and diffusion couples, were rapidly quenched in cold water in order to obtain the high temperature structure. The equilibrated phases and the diffusion zones were analysed using SEM/WDS spot analysis and line-scans. WDS line-scans were performed across diffusion zones with a spatial distance of ~1 μm to obtain the concentration profile of the three elements. Based on the phase equilibrium data from the solid-solid diffusion couples and key alloys obtained by SEM/WDS analysis, the isothermal section of the Ce-Mg-Zn phase diagram at 300 °C was constructed.

5. Conclusions

The Ce-Mg-Zn isothermal section at 300 °C was constructed for the whole composition range using diffusion couples and key alloy experiments. Most of the ternary compounds and extended binary

compounds have wide homogeneity ranges. The solid solutions in the system seem to occur due to the mutual substitution between Mg and Zn.

Diffusion couple studies coupled with key alloys experiments provide a powerful tool in phase diagram determination. The diffusion couples of this system showed complex relationships, due to the dispersed morphologies. However, their understanding provided very valuable information, which would not be possible without preparing a large number of samples.

The fast interatomic diffusion between Mg and Zn atoms led to the consuming of Mg by the $CeMg_{12}$ end-member by a diffusion reaction to form Mg-Zn compounds in the matrix. As a result, pure Mg was freed from the $Ce(Mg,Zn)_{12}$ solid solution, and a series of ternary compounds with constant Ce concentration, indicating the Mg/Zn substitution, were observed.

The ternary solubility of Zn in the Ce-Mg compounds was found to increase with a decrease in Mg concentration. Accordingly, the ternary solid solubility of Zn in $CeMg_{12}$ and $CeMg_3$ was measured as 5.6 and 28.4 at.% Zn, respectively. Furthermore, the CeMg and CeZn showed a complete solid solubility. The complete solubility was confirmed by a diffusion couple made from CeMg and CeZn alloys.

Acknowledgments

This research was supported by funding from the Magnesium Strategic Research Network (MagNET) [21].

Author Contributions

Ahmad Mostafa, carried out the experiments and analysis of the results. Ahmad Mostafa and Mamoun Medraj prepared and revised the manuscript. Mamoun Medraj initiated and directed the project. He helped in the interpretation of the results and followed up on the progress step by step.

Conflicts of Interest

The authors declare no conflict of interest.

References

1. Huang, M.; Li, H.; Ding, H.; Ren, Y.; Qin, G.; Hao, S. Partial phase relationships of Mg-Zn-Ce system at 350 °C. *Trans*. *Nonferrous Met*. *Soc*. **2009**, *19*, 681–685.
2. Ghosh, P.; Mezbahul-Islam, M.; Medraj, M. Critical assessment and thermodynamic modeling of Mg–Zn, Mg–Sn, Sn–Zn and Mg–Sn–Zn systems. *Calphad* **2012**, *36*, 28–43.
3. Zhu, Y.M.; Morton, A.J.; Nie, J.F. Improvement in the age-hardening response of Mg–Y–Zn alloys by Ag additions. *Scr*. *Mater*. **2008**, *58*, 525–528.
4. Omori, G.; Matsuo, S.; Asada, H. Precipitation process in a Mg-Ce alloy. *Trans*. *J*. *Jpn*. *Inst*. *Metals* **1975**, *16*, 247–256.
5. Huang, M.-L.; Li, H.-X.; Ding, H.; Bao, L.; Ma, X.-B.; Hao, S.-M. Intermetallics and phase relations of Mg-Zn-Ce alloys at 400 °C. *Trans*. *Nonferrous Met*. *Soc*. **2012**, *22*, 539–545.

6. Kodentsov, A.; Bastin, G.; Loo, F. The diffusion couple technique in phase diagram determination. *J. Alloy Compd*. **2001**, *320*, 207–217.
7. Xu, H.; Du, Y.; Zhou, Z.; Jin, Z. Determination of phase diagrams using the diffusion couple technique. *Rare Metals* **2006**, *25*, 427–430.
8. Korolkov, A.M.; Saldau, Y.P. Solubility of Zn and Ce in Mg in the solid state. *Izv Sektora Fiz-Khim Anal*. **1946**, *16*, 295–306.
9. Melnik, E.V.; Kostina, M.F.; Yarmlyuk, Ya.P.; Zmii, O.F. Study of the magnesium-zinc-cerium and magnesium-zinc-calcium ternary systems. *Magnievye Splavy*. *Mater*. *Vses*. *Soveshch*. *Issled*. *Razrab*. *Primen*. *Magnievyhk Splavov* **1978**, 95–99.
10. Drits, M.E.; Drozdova, E.I.; Korolkova, I.G.; Kinzhibalo, V.V.; Tyvanchuk, A.T. Investigation of polythermal sections of the Mg-Zn-Ce system in the Mg-rich region. *Russ*. *Metall*. *(Metally)* **1989**, *2*, 195–197.
11. Kolitsch, U.; Bellen, P.; Kaesche, S.; Maccio, D.; Bochvar, N.; Liberov, Y.; Rogl, P. Cerium-magnesium-zinc. In *Ternary Alloys–A Comprehensive Compendium of Evaluated Constitutional Data and Phase Diagrams*; Effenberg, G., Petzow, G., Eds.; VCH Verlagsgesellscahft, MSI GmbH: Weinheim, Stuttgart, Germany, 2000; pp. 168–176.
12. Agarwal, R.; Fries, S.G.; Lukas, H.L.; Petzow, G.; Sommer, F.; Chart, T.G.; Effenberg, G. Assessment of the Mg-Zn system. *Zeitschrift für Metall*. **1992**, *83*, 216–223.
13. Kevorkov, D.; Pekguleryuz, M. Experimental study of the Ce-Mg-Zn phase diagram at 350 °C via diffusion couple techniques. *J. Alloy Compnd*. **2009**, *478*, 427–436.
14. Chiu, C.-N.; Gröbner, J.; Kozlov, A.; Schmid-Fetzer, R. Experimental study and thermodynamic assessment of ternary Mg–Zn–Ce phase relations focused on Mg-rich alloys. *Intermetallics* **2010**, *18*, 399–405.
15. Pavlyuk, V.; Marciniak, B.; Różycka-Sokołowska, E. The isothermal section of the phase diagram of Ce–Mg–Zn ternary system at 470 K. *Intermetallics* **2012**, *20*, 8–15.
16. Okamoto, H. Supplemental literature review of binary phase diagrams: Cs-In, Cs-K, Cs-Rb, Eu-In, Ho-Mn, K-Rb, Li-Mg, Mg-Nd, Mg-Zn, Mn-Sm, O-Sb, and Si-Sr. *J. Phase Equilib*. *Diffus*. **2013**, *34*, 251–263.
17. Callister, W.; Rethwisch, D. *Materials Science and Engineering: An Introduction*, 7th ed.; John Wiley & Sons, Inc.: New York, NY, USA, 2007.
18. Dybkov, V.I. *Growth Kinetics of Chemical Compound Layers*; Cambridge International Science Publishing: Cambridge, UK, 2004.
19. *Panalytical Software*, ver2.2b (2.2.2); Available online: http://www.panalytical.com (accessed on 26 May 2014).
20. Villars, P.; Calvert, L. *Pearson's Crystal Data, Crystal Structure Database for Inorganic Compounds*, 1.3 [CD-ROM]; ASM International: Materials Park, OH, USA, 2009.
21. MagNET. Available online: http://www.MagNET.ubc.ca (accessed on 22 May 2014).